

SIMULTANEOUS IDENTIFICATION AND DENOISING OF DYNAMICAL SYSTEMS*

JEFFREY M. HOKANSON[†], GIANLUCA IACCARINO[‡], AND ALIREZA DOOSTAN[†]

Abstract. In recent years there has been a push to discover the governing equations dynamical systems directly from measurements of the state, often motivated by systems that are too complex to directly model. Although there has been substantial work put into such a discovery, doing so in the case of large noise has proved challenging. Here we develop an algorithm for Simultaneous Identification and Denoising of a Dynamical System (SIDDS). We infer the noise in the state measurements by requiring that the denoised data satisfies the dynamical system with an equality constraint. This is unlike existing work where the mismatch in the dynamical system is treated as a penalty in the objective. We assume the dynamics is represented in a pre-defined basis and develop a sequential quadratic programming approach to solve the SIDDS problem featuring a direct solution of KKT system with a specialized preconditioner. In addition, we show how we can include sparsity promoting regularization using an iteratively reweighted least squares approach. The resulting algorithm leads to estimates of the dynamical system that approximately achieve the Cramér-Rao lower bound and, with sparsity promotion, can correctly identify the sparsity structure for higher levels of noise than existing techniques. Moreover, because SIDDS decouples the data from the evolution of the dynamical system, we show how to modify the problem to accurately identify systems from low sample rate measurements. The inverse problem approach and solution framework used by SIDDS has the potential to be expanded to related problems identifying governing equations from noisy data.

Key words. inverse problem, parameter estimation, data-driven discovery,

AMS subject classifications. 34A55, 65L09, 90C55, 93B30

DOI.

1. Introduction. Here we consider the problem of identifying a dynamical system from measurements of its state. Suppose the state of this system $\mathbf{x} \in \mathbb{R}^d$ satisfies a first order, autonomous ordinary differential equation (ODE)

$$(1.1) \quad \begin{cases} \dot{\mathbf{x}}(t) = \mathbf{f}(\mathbf{x}(t)), \\ \mathbf{x}(0) = \mathbf{x}_0, \end{cases} \quad \text{where } \mathbf{f} : \mathbb{R}^d \rightarrow \mathbb{R}^d.$$

Our goal is to identify the function \mathbf{f} from m measurements of the state $\{\mathbf{x}(t_j)\}_{j=1}^m$ at times $\{t_j\}_{j=1}^m$. This problem can emerge in a variety of contexts from model reduction to system identification. Here we consider the case where we cannot directly access $\mathbf{x}(t_j)$, but instead can only access a noisy measurement $\mathbf{y}_j \approx \mathbf{x}(t_j)$.

1.1. Parameterization. An important choice for recovering the operator \mathbf{f} is its parameterization. Here, we express \mathbf{f} as a sum of n scalar-valued basis functions $\phi_k : \mathbb{R}^d \rightarrow \mathbb{R}$ with corresponding coefficients $\mathbf{c}_k \in \mathbb{R}^d$ following [6]

$$(1.2) \quad \mathbf{f}(\mathbf{x}; \mathbf{C}) := \sum_{k=1}^n \mathbf{c}_k \phi_k(\mathbf{x}), \quad \text{where } \mathbf{C} := \begin{bmatrix} \mathbf{c}_1^\top \\ \vdots \\ \mathbf{c}_n^\top \end{bmatrix} \in \mathbb{R}^{n \times d}.$$

*Submitted to the editors DATE.

Funding: This material is based upon work supported by the Department of Energy, National Nuclear Security Administration under Award Number DE-NA0003968.

[†] Department of Aerospace Engineering Sciences, University of Colorado at Boulder, Boulder, CO 80309 (jeffrey@hokanson.us, alireza.doostan@colorado.edu)

[‡] Center for Turbulence Research, Stanford University, Stanford, CA 94305 (jops@stanford.edu)

Typically $\{\phi_k\}_{k=1}^m$ is chosen to represent a polynomial basis; i.e. when $d = 2$ a total degree-2 basis would be,

$$\phi_1(\mathbf{x}) = 1 \quad \phi_2(\mathbf{x}) = x_1 \quad \phi_3(\mathbf{x}) = x_2 \quad \phi_4(\mathbf{x}) = x_1^2 \quad \phi_5(\mathbf{x}) = x_1 x_2 \quad \phi_6(\mathbf{x}) = x_2^2;$$

however non-polynomial terms such as $\phi_k(\mathbf{x}) = \sin(x_1)$ can also be incorporated. In some cases, we will further seek a parsimonious, interpretable expression for \mathbf{f} by seeking a sparse coefficient matrix \mathbf{C} . Note, however, that there are other parameterizations possible for \mathbf{f} , such as a neural network [28].

1.2. A Naive Least Squares Approach. A variety of methods exploit a simple linear relationship to estimate the coefficients \mathbf{C} . Suppose we have access to exact measurements of the state $\mathbf{x}(t_j)$ and its derivative $\dot{\mathbf{x}}(t_j)$ and stack these into matrices

$$(1.3) \quad \mathbf{X} := \begin{bmatrix} \mathbf{x}(t_1)^\top \\ \vdots \\ \mathbf{x}(t_m)^\top \end{bmatrix} \in \mathbb{R}^{m \times d} \quad \text{and} \quad \dot{\mathbf{X}} := \begin{bmatrix} \dot{\mathbf{x}}(t_1)^\top \\ \vdots \\ \dot{\mathbf{x}}(t_m)^\top \end{bmatrix} \in \mathbb{R}^{m \times d}.$$

Further, we build the matrix-valued function $\Phi : \mathbb{R}^{m \times d} \rightarrow \mathbb{R}^{m \times n}$ containing the evaluations of the basis functions:

$$(1.4) \quad \Phi(\mathbf{X}) := \begin{bmatrix} \phi_1(\mathbf{x}(t_1)) & \cdots & \phi_n(\mathbf{x}(t_1)) \\ \vdots & & \vdots \\ \phi_1(\mathbf{x}(t_m)) & \cdots & \phi_n(\mathbf{x}(t_m)) \end{bmatrix} \in \mathbb{R}^{m \times n}.$$

With this notation, based on the differential equation (1.1) and the expansion in (1.2), the coefficients \mathbf{C} must satisfy the linear system:

$$(1.5) \quad \dot{\mathbf{X}} = \begin{bmatrix} \dot{\mathbf{x}}(t_1)^\top \\ \vdots \\ \dot{\mathbf{x}}(t_m)^\top \end{bmatrix} = \begin{bmatrix} \mathbf{f}(\mathbf{x}(t_1))^\top \\ \vdots \\ \mathbf{f}(\mathbf{x}(t_m))^\top \end{bmatrix} = \begin{bmatrix} \sum_{k=1}^n \mathbf{c}_k^\top \phi_k(\mathbf{x}(t_1)) \\ \vdots \\ \sum_{k=1}^n \mathbf{c}_k^\top \phi_k(\mathbf{x}(t_m)) \end{bmatrix} = \Phi(\mathbf{X})\mathbf{C}.$$

When this problem is well-posed, there is a unique solution for \mathbf{C} given $\dot{\mathbf{X}}$ and $\Phi(\mathbf{X})$; numerically, \mathbf{C} can be identified by solving a least squares problem

$$(1.6) \quad \min_{\mathbf{C} \in \mathbb{R}^{n \times d}} \|\dot{\mathbf{X}} - \Phi(\mathbf{X})\mathbf{C}\|_F^2,$$

where $\|\cdot\|_F$ denotes the Frobenius norm. However, $\Phi(\mathbf{X})$ need not necessarily be full-rank; for example, if there is a linear combination of basis functions encoding a conservation law for the system, then $\Phi(\mathbf{X})$ will have a nontrivial nullspace.

The limitations of experimental measurements present two difficulties: we may not have access to the derivative $\dot{\mathbf{x}}(t_j)$ and our measurements \mathbf{y}_j of $\mathbf{x}(t_j)$ are invariably contaminated by noise. We can correct the former difficulty by estimating the derivative using finite-difference approximations based on measurements \mathbf{y}_j . When measurements are uniformly spaced in time with time-step δ , e.g., $t_j = \delta(j-1)$, we can build a finite difference matrix $\mathbf{D} \in \mathbb{R}^{m \times m}$ using a q -point central difference rule in the interior and an order $q-1$ accurate rule on the boundary. For example, a

3-point finite difference matrix is

$$(1.7) \quad \mathbf{D} = \frac{1}{2\delta} \begin{bmatrix} -3 & 4 & -1 & & & \\ -1 & 0 & 1 & & & \\ & \ddots & \ddots & \ddots & & \\ & & \ddots & \ddots & \ddots & \\ & & & -1 & 0 & 1 \\ & & & 1 & -4 & 3 \end{bmatrix} \in \mathbb{R}^{m \times m}.$$

This provides the derivative approximation $\dot{\mathbf{X}} \approx \mathbf{D}\mathbf{X}$. To deal with the other difficulty of only having access to noisy measurements \mathbf{y}_j of $\mathbf{x}(t_j)$, we can replace \mathbf{X} with \mathbf{Y} :

$$(1.8) \quad \mathbf{X} \approx \mathbf{Y} := \begin{bmatrix} \mathbf{y}_1^\top \\ \vdots \\ \mathbf{y}_m^\top \end{bmatrix} \in \mathbb{R}^{m \times d}$$

Thus making the substitutions $\dot{\mathbf{X}} \approx \mathbf{D}\mathbf{X} \approx \mathbf{D}\mathbf{Y}$ and $\Phi(\mathbf{X}) \approx \Phi(\mathbf{Y})$, we can infer the coefficients \mathbf{C} by solving the least squares problem

$$(1.9) \quad \min_{\mathbf{C} \in \mathbb{R}^{n \times d}} \|\mathbf{D}\mathbf{Y} - \Phi(\mathbf{Y})\mathbf{C}\|_{\text{F}}^2.$$

We refer to this as *Least Squares Operator Inference* (LSOI), and this problem appears as a component in many approaches.

Although LSOI is inexpensive to solve, it inherits many limitations from the chain of approximations used in its construction. The noise in \mathbf{Y} may be amplified through the nonlinear basis functions in Φ and the derivative estimate $\mathbf{D}\mathbf{Y}$ may be similarly inaccurate due to noise. Thus when LSOI appears, it is often coupled with techniques to ameliorate these issues. For example *Sparse Identification of Nonlinear Dynamics* (SINDy) [6] introduces the desire for a sparse coefficient matrix \mathbf{C} . This sparsity promotion improves the conditioning of the linear system by (effectively) deleting columns from $\Phi(\mathbf{Y})$ [20, Cor. 7.3.6]. Another corrective measure is to find a better estimate of \mathbf{X} by applying a denoising technique to the data \mathbf{Y} to obtain an estimate $\hat{\mathbf{Y}}$ that replaces \mathbf{Y} in LSOI (1.9). When $\hat{\mathbf{Y}}$ is a better estimate of \mathbf{X} than the original data \mathbf{Y} , this improves estimate of \mathbf{C} ; however careful tuning is needed to avoid either over smoothing or insufficiently removing noise [10]. The only place where LSOI appears without embellishment is in model reduction [27, eq. (12)] where the data $\{\mathbf{y}_j\}_{j=1}^m$ is not contaminated with noise.

1.3. Identification and Denoising. A fundamental limitation of LSOI is that, in the presence of noise, the coefficient estimates do not satisfy the discretized dynamics; that is, $\mathbf{D}\mathbf{Y} \neq \Phi(\mathbf{Y})\mathbf{C}$. Our key contribution is to introduce an auxiliary variable \mathbf{Z} which *will* satisfy the discretized dynamics exactly: $\mathbf{D}\mathbf{Z} = \Phi(\mathbf{Z})\mathbf{C}$. Then we minimize the mismatch between \mathbf{Z} and the data \mathbf{Y} in an appropriate norm. If we assume noise follows independent and identically distributed normal distribution where $\mathbf{y}_j \sim \mathcal{N}(\mathbf{x}(t_j), \sigma^2 \mathbf{I})$, then we solve the constrained optimization problem

$$(1.10) \quad \begin{aligned} \min_{\mathbf{C} \in \mathbb{R}^{n \times d}, \mathbf{Z} \in \mathbb{R}^{m \times d}} \quad & \|\mathbf{Y} - \mathbf{Z}\|_{\text{F}}^2 \\ \text{s.t.} \quad & \mathbf{D}\mathbf{Z} = \Phi(\mathbf{Z})\mathbf{C}. \end{aligned}$$

We call this *Simultaneous Identification and Denoising of Dynamical Systems* (SIDDS).

Although we have derived SIDDS using a similar framework to LSOI, SIDDS can alternatively be derived from a more traditional inverse problem approach, see, e.g. [17], where SIDDS approximates the solution of the differential equation constrained optimization problem

$$(1.11) \quad \min_{\mathbf{C} \in \mathbb{R}^{n \times d}, \mathbf{z}_0 \in \mathbb{R}^d} \sum_{j=1}^m \|\mathbf{y}_j - \boldsymbol{\zeta}(t_j)\|_2^2$$

$$\text{s.t. } \dot{\boldsymbol{\zeta}}(t) = \mathbf{f}(\boldsymbol{\zeta}(t); \mathbf{C}), \quad \boldsymbol{\zeta}(0) = \mathbf{z}_0.$$

In particular, SIDDS uses the *discretize-then-optimize* approach to discretize (1.11) in time yielding (1.10). SIDDS also solves a full-space optimization problem [16] for both the coefficients \mathbf{C} and the state history $\mathbf{z}_j = \boldsymbol{\zeta}(t_j)$. An alternative would be to use a reduced-space formulation [18] where $\boldsymbol{\zeta}$ is implicitly defined by \mathbf{C} and \mathbf{z}_0

$$(1.12) \quad \min_{\mathbf{C} \in \mathbb{R}^{n \times d}, \mathbf{z}_0 \in \mathbb{R}^d} \sum_{j=1}^m \|\mathbf{y}_j - \boldsymbol{\zeta}(t_j; \mathbf{C}, \mathbf{z}_0)\|_2^2, \quad \text{where} \quad \begin{cases} \dot{\boldsymbol{\zeta}}(t; \mathbf{C}, \mathbf{z}_0) = \mathbf{f}(\boldsymbol{\zeta}(t); \mathbf{C}), \\ \boldsymbol{\zeta}(0; \mathbf{C}, \mathbf{z}_0) = \mathbf{z}_0. \end{cases}$$

Although the reduced-space approach allows solving a smaller, unconstrained optimization problem compared to the full-space approach, the reduced-space objective presents challenges. When approximating chaotic systems, small changes in \mathbf{C} can yield exponentially increasing changes in $\boldsymbol{\zeta}(t; \mathbf{C}, \mathbf{z}_0)$ as t increases. This hypersensitivity, in turn, means that local information, such as gradients and Hessians, are not accurate beyond some small neighborhood. This makes finding a meaningful descent direction challenging. In contrast, the full-space approach in SIDDS has a convex objective with constraints that only need be satisfied at the final optimization iteration.

The SIDDS problem shares similarities with problems in data assimilation [2]. Like data assimilation, we seek to estimate the true state from noisy measurements, and as in some formulations, we seek to estimate the parameters of the underlying differential equation. Unlike SIDDS which is solved using a full space method, most data assimilation algorithms use a reduced space approach due to scaling concerns which is a poor choice in our setting due to the hypersensitivity discussed above.

1.4. A First Example. Why use SIDDS instead of the existing approaches based on LSOI? In short, SIDDS recovers far more accurate dynamical systems from noisy measurements. As a first example, consider the simple harmonic oscillator $\ddot{x}(t) = -x(t)$ in first order form:

$$(1.13) \quad \begin{bmatrix} \dot{x}_1 \\ \dot{x}_2 \end{bmatrix} = \begin{bmatrix} 0 & 1 \\ -1 & 0 \end{bmatrix} \begin{bmatrix} x_1 \\ x_2 \end{bmatrix} \quad \text{with} \quad \begin{bmatrix} x_1(0) \\ x_2(0) \end{bmatrix} = \begin{bmatrix} 1 \\ 0 \end{bmatrix}.$$

Reconstructing this system, we use two linear basis functions: $\phi_1(\mathbf{x}) = x_1$ and $\phi_2(\mathbf{x}) = x_2$. Then if we take $m = 2000$ measurements with sample rate $\delta = 10^{-2}$ that are contaminated with i.i.d. standard normal noise with unit covariance, using the 3-point derivative approximation in (1.7), we recover the systems

LSOI	SIDDS
$\begin{bmatrix} \dot{x}_1 \\ \dot{x}_2 \end{bmatrix} = \begin{bmatrix} -0.23580696 & 2.85537791 \\ -2.60758784 & 0.2062968 \end{bmatrix} \begin{bmatrix} x_1 \\ x_2 \end{bmatrix}$	$\begin{bmatrix} \dot{x}_1 \\ \dot{x}_2 \end{bmatrix} = \begin{bmatrix} -0.01155883 & 0.99851078 \\ -1.0097105 & -0.0019787 \end{bmatrix} \begin{bmatrix} x_1 \\ x_2 \end{bmatrix}.$

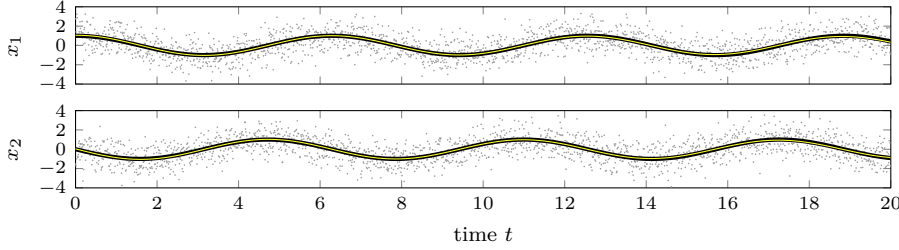


FIG. 1.1. For the simple harmonic oscillator example, SIDDS is able to accurately denoise the state and recover the dynamical system. Here the true system evolution is shown as a black line, the measured data as gray points, and the recovered system as a yellow line.

Here SIDDS's estimate is accurate to 2-significant figures; LSOI captures none!

The reason why SIDDS performs so much better than LSOI is that, subject to optimization algorithm finding the correct minimizer, \mathbf{Z} is a maximum likelihood estimate of the true data \mathbf{X} so that $\mathbf{Z} \approx \mathbf{X}$ as illustrated in Figure 1.1. With this accurate estimate of \mathbf{X} in \mathbf{Z} , SIDDS provides an accurate estimate of the coefficients \mathbf{C} . In contrast, LSOI does not provide a maximum likelihood estimate of \mathbf{C} due to the way it correlates noise in the expression $\mathbf{D}\mathbf{Y} - \Phi(\mathbf{Y})\mathbf{C}$. Details concerning these results are provided in section 3.

1.5. Sparsity Promotion. With an eye to obtain an easily interpretable expansion of \mathbf{f} in the basis $\{\phi_k\}_{k=1}^n$ as in (1.2), it is common to apply a regularization to encourage the coefficients \mathbf{C} to be sparse. *Sparse Identification of Nonlinear Dynamics* (SINDy) encompasses a variety of algorithms using different techniques to promote sparsity in \mathbf{C} , many inspired by compressed sensing. For example, Sequentially Thresholded Least Squares (STLS) (see, e.g., [5]) can be used iteratively to remove small coefficients in \mathbf{C} [6]. Another approach is to add an ℓ_p -norm regularization term to the objective, i.e.,

$$(1.14) \quad \min_{\mathbf{C}} \|\mathbf{D}\mathbf{Y} - \Phi(\mathbf{Y})\mathbf{C}\|_{\mathbb{F}}^2 + \lambda R_p(\text{vec}(\mathbf{C})) \quad \text{where} \quad R_p(\mathbf{w}) := \begin{cases} \|\mathbf{w}\|_p^p, & p > 0; \\ \|\mathbf{w}\|_0, & p = 0; \end{cases}$$

where $\text{vec}(\cdot)$ denotes row-major vectorization and $\|\mathbf{w}\|_0$ is the number of nonzero entries in \mathbf{w} . This is a nonconvex problem for $p < 1$ and nondifferentiable for $p = 0$; however, in many applications small values of p , especially $p = 0$, provide better recovery. There are a variety of techniques that can be used to solve (1.14), such as Iteratively Reweighted Least Squares (IRLS) [4, Subsec. 4.5.2] or Iteratively Reweighted ℓ_1 -norm ($\text{IR}\ell_1$) [7]. The latter is used for recovering dynamical systems in [9] with an accuracy better than that of STLS. Our approach with SIDDS will be to promote sparsity by adding a similar regularization penalty

$$(1.15) \quad \begin{aligned} & \min_{\mathbf{C}, \mathbf{Z}} \|\mathbf{Y} - \mathbf{Z}\|_{\mathbb{F}}^2 + \alpha R_p(\text{vec}(\mathbf{C})) \\ & \text{s.t. } \mathbf{D}\mathbf{Z} = \Phi(\mathbf{Z})\mathbf{C}. \end{aligned}$$

We refer to this variant as $\text{SIDDS} + \ell_p$. In our numerical experiments, we often choose $p = 0$ and use regularized IRLS [8] to provide a quadratic approximation of R_p .

Although these sparsity promoting techniques will often regularize the problem and reduce the impact of noise, simply identifying the correct sparsity structure is not

sufficient to obtain an accurate parameter estimate when using the LSOI objective. Returning to the simple harmonic oscillator example in (1.13), if we fix the correct sparsity structure for both of these methods, we obtain

$$\begin{array}{cc} \text{LSOI + fixed sparsity} & \text{SIDDS + fixed sparsity} \\ \begin{bmatrix} x'_1 \\ x'_2 \end{bmatrix} = \begin{bmatrix} 0 & 7.15983089 \\ -5.69559158 & 0 \end{bmatrix} \begin{bmatrix} x_1 \\ x_2 \end{bmatrix} & \begin{bmatrix} x'_1 \\ x'_2 \end{bmatrix} = \begin{bmatrix} 0 & 0.99695336 \\ -1.01100718 & 0 \end{bmatrix} \begin{bmatrix} x_1 \\ x_2 \end{bmatrix}. \end{array}$$

Hence fixing the sparsity pattern—equivalent to hard thresholding in STLS—has not improved the parameter estimate using LSOI. Thus sparsity promoting regularization is not sufficient to ensure a method with an LSOI objective term will provide an accurate estimate. Instead, some effort must be applied to remove noise from measurements \mathbf{Y} so that an accurate estimate of \mathbf{C} may be obtained.

1.6. Existing Denoising Work. There are a wide variety of algorithms for identifying sparse dynamics. We focus our attention on those methods, like ours, that estimate the true state and coefficients simultaneously; often this is stated equivalently as estimating the measurement noise. For the most part, these methods do so by adding a penalty based on the dynamical system mismatch rather than adding an equality constraint as with SIDDS. Beyond these methods, there are a variety of techniques that separately denoise measurements and then apply LSOI or related algorithm; see, e.g., [10]. Although these yield improved performance in the presence of noise, their use requires careful parameter tuning. Hence, we leave a more thorough comparison to future work.

1.6.1. Sparse Corruption. Related to our case where all measurements have been corrupted by noise, is the case where an unknown (small) fraction of measurements are contaminated by noise. If $\mathbf{Y} - \mathbf{X}$ has only a few nonzero rows, the dynamical system constraint will be satisfied except for a few nonzero rows; if $\mathbf{DX} = \Phi(\mathbf{X})\mathbf{C}$, then the constraint mismatch \mathbf{E} satisfies

$$(1.16) \quad \mathbf{E} = \Phi(\mathbf{Y})\mathbf{C} - \mathbf{DY} = \Phi(\mathbf{Y} - \mathbf{X})\mathbf{C} - \mathbf{D}(\mathbf{Y} - \mathbf{X}).$$

Tran and Ward [31] propose identifying these corrupted measurements and a sparse dynamical system by solving

$$(1.17) \quad \begin{aligned} \min_{\mathbf{C} \in \mathbb{R}^{n \times d}, \mathbf{E} \in \mathbb{R}^{m \times d}} \quad & \sum_j \|\mathbf{E}_{j,\cdot}\|_2 \\ \text{s.t. } & \mathbf{DY} + \mathbf{E} = \Phi(\mathbf{Y})\mathbf{C} \quad \text{and } \mathbf{C} \text{ sparse} \end{aligned}$$

where $\mathbf{E}_{j,\cdot}$ represents the j th row of \mathbf{E} . Here the objective encodes an ℓ_1 convex relaxation of the ℓ_0 -norm to encourage sparsity in \mathbf{E} . Although this method does identify the corrupted measurements, unlike our work, it does not identify a corrected state and avoids the nonlinearity in Φ , working with a fixed $\Phi(\mathbf{Y})$ rather than our $\Phi(\mathbf{Z})$.

1.6.2. Modified SINDy. Modified SINDy [21] introduces a variable \mathbf{N} to estimate the noise, and penalizes violation of the dynamical system constraint by the denoised state. Introducing the evolution operator $\mathcal{E}^t(\mathbf{x}, \mathbf{C})$ that advances the differential equation with coefficients \mathbf{C} from initial condition \mathbf{x} ,

$$(1.18) \quad \mathcal{E}^t : \mathbb{R}^d \times \mathbb{R}^{n \times d} \rightarrow \mathbb{R}^d, \quad \mathcal{E}^t(\zeta_0, \mathbf{C}) := \zeta(t), \quad \text{where} \quad \begin{cases} \dot{\zeta}(t) = \mathbf{f}(\zeta(t); \mathbf{C}), \\ \zeta(0) = \zeta_0, \end{cases}$$

Modified SINDy solves for some integer $q \geq 1$
(1.19)

$$\min_{\substack{\mathbf{C} \in \mathbb{R}^{n \times d} \\ \mathbf{N} \in \mathbb{R}^{m \times d}}} \|\mathbf{D}(\mathbf{Y} - \mathbf{N}) - \Phi(\mathbf{Y} - \mathbf{N})\mathbf{C}\|_F^2 + \sum_{j=q+1}^{M-q} \sum_{\substack{i=-q \\ i \neq 0}}^q \omega_i \|\mathbf{y}_{j+i} - \mathbf{n}_{j+i} - \mathcal{E}^{\delta i}(\mathbf{y}_j - \mathbf{n}_j, \mathbf{C})\|_2^2$$

where $\omega_i > 0$ is a weight. Their implementation alternates between minimizing the objective above using stochastic, gradient-based optimization and using STLS to identify a sparsity structure in \mathbf{C} . A similar approach was used in [28] where \mathbf{f} was approximated by a neural network.

Although more accurate than LSOI, this approach is suboptimal because it imposes the dynamical system constraint through a penalty rather than as an equality constraint. We can observe this loss of accuracy in the simple harmonic oscillator example; with their implementation of Modified SINDy we recover

Modified SINDy	SIDDS+ ℓ_0
$\begin{bmatrix} \dot{x}_1 \\ \dot{x}_2 \end{bmatrix} = \begin{bmatrix} 0 & 0.91451177 \\ -1.10430015 & 0 \end{bmatrix} \begin{bmatrix} x_1 \\ x_2 \end{bmatrix}$	$\begin{bmatrix} \dot{x}_1 \\ \dot{x}_2 \end{bmatrix} = \begin{bmatrix} 0 & 0.99695336 \\ -1.01100718 & 0 \end{bmatrix} \begin{bmatrix} x_1 \\ x_2 \end{bmatrix}$

Although Modified SINDy vastly outperforms LSOI, the coefficient error is an order of magnitude larger than SIDDS.

1.6.3. Physics Informed Spline Learning. Physics Informed Spline Learning (PiSL) [30] uses a similar approach to Modified SINDy, adding a penalty for violating the dynamical system constraint. In PiSL, the estimated state $\mathbf{z}(t)$ is expressed in a cubic spline basis, $\mathbf{z}(t) = \mathbf{T}(t)\mathbf{P}$ where $\mathbf{T}(t)$ is a cubic spline basis and \mathbf{P} are the control points. To identify the dynamical system, PiSL solves [30, eq. (9)]

$$(1.20) \quad \min_{\mathbf{P}, \mathbf{C}} \frac{1}{m} \sum_{j=1}^m \|\mathbf{y}_j - \mathbf{T}(t_j)\mathbf{P}\|_2^2 + \frac{\alpha}{m} \sum_{j=1}^m \|\dot{\mathbf{T}}(t_j)\mathbf{P} - \sum_{k=1}^n \mathbf{c}_k \phi(\mathbf{T}(t_j)\mathbf{P})\|_2^2 + \beta \|\mathbf{C}\|_0$$

(we omit the stochastic subsampling used in the first two terms in the objective). PiSL's implementation uses a similar approach to Modified SINDy: an alternating optimization between minimizing \mathbf{P} and \mathbf{C} with a fixed sparsity structure and then applying STLS to identify the sparsity pattern in \mathbf{C} . Although this method uses a different basis and differs in some details, the overall approach is similar to Modified SINDy.

1.7. Overview. The remainder of this manuscript is dedicated to two questions: what is the statistical performance of SIDDS and how can we efficiently solve the SIDDS optimization problem. We begin by introducing vectorization notation in section 2 replacing the matrix-valued constraints with vector-valued constraints. Then in section 3 we derive the asymptotic estimates of the performance of different algorithms. We first establish the optimal covariance using the constrained Cramér-Rao Lower Bound (CRLB) and then estimate the covariance of LSOI and SIDDS. Our numerical experiments show that SIDDS obtains the CRLB upto discretization error whereas LSOI does not. Sections 4 and 5 describe how to efficiently implement SIDDS; section 4 discusses an IRLS approximation to the ℓ_p -norm regularization and initialization while Section 5 discusses the details of how to efficiently solve SIDDS using a sequential quadratic programming (SQP) approach using a preconditioned MINRES iteration. Finally in section 6, we provide a number of numerical experiments comparing the performance of SIDDS and SIDDS+ ℓ_0 to LSOI, STLS, and

Modified SINDy. These experiments show that SIDDS almost exactly obtains the CRLB unlike existing techniques. Moreover, SIDDS+ ℓ_0 can accurately recover the sparsity structure in \mathbf{C} for higher levels of noise than other methods. We conclude with a brief discussion in section 7 of variants of SIDDS for related problems for identifying dynamical systems from measurements.

1.8. Reproducibility. Following the principles of reproducible research, software implementing our algorithms and the scripts to generate data in the figures are available at <http://github.com/jeffrey-hokanson/sidds>.

2. Notation and Derivatives. To follow standard practice in optimization, we reformulate the SIDDS optimization problem with a vector-valued objective and constraint which simplifies the derivations that follow. In this section, we introduce notation for these vectorized quantities and the constraint derivative.

2.1. Vectorization. Throughout, we use the row-major vectorization operator

$$(2.1) \quad \text{vec} : \mathbb{R}^{m \times d} \rightarrow \mathbb{R}^{md}, \quad \text{vec}(\mathbf{X}) = \text{vec} \left(\begin{bmatrix} \mathbf{x}_1^\top \\ \vdots \\ \mathbf{x}_m^\top \end{bmatrix} \right) := \begin{bmatrix} \mathbf{x}_1 \\ \vdots \\ \mathbf{x}_m \end{bmatrix}.$$

For brevity, vectorized matrices are denoted by the corresponding lower case letter annotated with a harpoon; e.g.,

$$(2.2) \quad \vec{\mathbf{x}} := \text{vec}(\mathbf{X}), \quad \vec{\mathbf{y}} := \text{vec}(\mathbf{Y}), \quad \vec{\mathbf{z}} := \text{vec}(\mathbf{Z}), \quad \vec{\mathbf{c}} := \text{vec}(\mathbf{C}).$$

Quantities that are still matrices after vectorization are denoted by uppercase letters annotated with a harpoon; e.g.,

$$(2.3) \quad \text{vec}(\Phi(\mathbf{Z})\mathbf{C}) = \vec{\Phi}(\vec{\mathbf{z}})\vec{\mathbf{c}}, \quad \vec{\Phi}(\vec{\mathbf{z}}) := \Phi(\vec{\mathbf{z}}) \otimes \mathbf{I}_d,$$

$$(2.4) \quad \text{vec}(\mathbf{DZ}) = \vec{\mathbf{D}}\vec{\mathbf{z}}, \quad \vec{\mathbf{D}} := \mathbf{D} \otimes \mathbf{I}_d,$$

where \otimes denotes the Kronecker product and $\mathbf{I}_d \in \mathbb{R}^{d \times d}$ denotes the identity. The choice of row-major vectorization is important so that $\vec{\mathbf{D}}$ has low bandwidth. If \mathbf{D} uses a q -point stencil, then $\vec{\mathbf{D}}$ has bandwidth $d(q-1)$. With this vectorized notation, we can rewrite the SIDDS+ ℓ_p problem as

$$(2.5) \quad \begin{aligned} \min_{\vec{\mathbf{c}} \in \mathbb{R}^{dn}, \vec{\mathbf{z}} \in \mathbb{R}^{dm}} \quad & \|\vec{\mathbf{y}} - \vec{\mathbf{z}}\|_2^2 + \alpha R_p(\vec{\mathbf{c}}) \\ \text{s.t.} \quad & \vec{\mathbf{D}}\vec{\mathbf{z}} = \vec{\Phi}(\vec{\mathbf{z}})\vec{\mathbf{c}} \end{aligned}$$

since $\|\vec{\mathbf{Y}} - \vec{\mathbf{Z}}\|_F^2 = \|\text{vec}(\vec{\mathbf{Y}} - \vec{\mathbf{Z}})\|_2^2 = \|\vec{\mathbf{y}} - \vec{\mathbf{z}}\|_2^2$.

2.2. Constraint Derivative. The constraint derivative appears in several parts of our analysis;

$$(2.6) \quad \vec{\mathbf{h}}(\vec{\mathbf{c}}, \vec{\mathbf{z}}) := \vec{\mathbf{D}}\vec{\mathbf{z}} - \vec{\Phi}(\vec{\mathbf{z}})\vec{\mathbf{c}},$$

$$(2.7) \quad \nabla \vec{\mathbf{h}}(\vec{\mathbf{c}}, \vec{\mathbf{z}}) = [\nabla_{\vec{\mathbf{c}}} \vec{\mathbf{h}}(\vec{\mathbf{c}}, \vec{\mathbf{z}}) \quad \nabla_{\vec{\mathbf{z}}} \vec{\mathbf{h}}(\vec{\mathbf{c}}, \vec{\mathbf{z}})] = [-\vec{\Phi}(\vec{\mathbf{z}}) \quad \vec{\mathbf{D}} - \nabla_{\vec{\mathbf{z}}}[\vec{\Phi}(\vec{\mathbf{z}})\vec{\mathbf{c}}]].$$

The last term merits some elaboration. The gradient of $\vec{\Phi}$ is the 3-tensor $\nabla \vec{\Phi} : \mathbb{R}^{dm} \rightarrow \mathbb{R}^{(dm) \times (dn) \times (dm)}$; thus a Taylor series expansion of $\vec{\Phi}$ about $\vec{\mathbf{z}}$ is

$$(2.8) \quad \vec{\Phi}(\vec{\mathbf{z}} + \delta \vec{\mathbf{z}}) = \vec{\Phi}(\vec{\mathbf{z}}) + \nabla \vec{\Phi}(\vec{\mathbf{z}}) \bar{\times}_3 \delta \vec{\mathbf{z}} + \mathcal{O}(\|\delta \vec{\mathbf{z}}\|_2^2),$$

where $\bar{\times}_3$ denotes tensor multiplication along the third tensor mode [24, subsec. 2.5]. If we take the same Taylor expansion for $\bar{\Phi}(\bar{\mathbf{z}})\bar{\mathbf{c}}$,

$$(2.9) \quad \bar{\Phi}(\bar{\mathbf{z}} + \bar{\delta\mathbf{z}})\bar{\mathbf{c}} = \bar{\Phi}(\bar{\mathbf{z}})\bar{\mathbf{c}} + \left[\nabla \bar{\Phi}(\bar{\mathbf{z}}) \bar{\times}_3 \bar{\delta\mathbf{z}} \right] \bar{\mathbf{c}} + \mathcal{O}(\|\bar{\delta\mathbf{z}}\|_2^2),$$

we can interchange the order of tensor multiplication yielding

$$(2.10) \quad \bar{\Phi}(\bar{\mathbf{z}} + \bar{\delta\mathbf{z}})\bar{\mathbf{c}} = \bar{\Phi}(\bar{\mathbf{z}})\bar{\mathbf{c}} + \left[\nabla \bar{\Phi}(\bar{\mathbf{z}}) \bar{\times}_2 \bar{\mathbf{c}} \right] \bar{\delta\mathbf{z}} + \mathcal{O}(\|\bar{\delta\mathbf{z}}\|_2^2).$$

Hence the derivative of $\bar{\Phi}(\bar{\mathbf{z}})\bar{\mathbf{c}}$ with respect to $\bar{\mathbf{z}}$ is

$$(2.11) \quad \nabla_{\bar{\mathbf{z}}}[\bar{\Phi}(\bar{\mathbf{z}})\bar{\mathbf{c}}] = \nabla \bar{\Phi}(\bar{\mathbf{z}}) \bar{\times}_2 \bar{\mathbf{c}} \in \mathbb{R}^{(dm) \times (dm)}.$$

This expression allows us to reduce the memory required to compute the constraint derivative; our implementation never explicitly forms the large 3-tensor $\nabla \bar{\Phi}(\bar{\mathbf{z}})$, but instead builds $\nabla \bar{\Phi}(\bar{\mathbf{z}}) \bar{\times}_2 \bar{\mathbf{c}}$ directly.

3. Statistical Performance. A key question is: how do methods like SIDDS and LSOI perform when measurements are contaminated by noise? In this section, we analyze these methods when measurements $\bar{\mathbf{y}}$ have been contaminated with normally distributed additive noise $\bar{\mathbf{n}}$ with zero mean and full-rank covariance $\bar{\Sigma}$,

$$(3.1) \quad \bar{\mathbf{y}} = \bar{\mathbf{x}} + \bar{\mathbf{n}}, \quad \bar{\mathbf{n}} \sim \mathcal{N}(\bar{\mathbf{0}}, \bar{\Sigma}); \quad \text{equivalently, } \bar{\mathbf{y}} \sim \mathcal{N}(\bar{\mathbf{x}}, \bar{\Sigma}).$$

For these methods, we estimate how $\bar{\mathbf{c}}$ is perturbed in the limit of small noise and compute the mean and variance of $\bar{\mathbf{c}}$ asymptotically. Although only asymptotically valid, numerical experiments show these estimates provide reliable guides to performance. To begin, we compute a lower bound on the covariance of $\bar{\mathbf{c}}$ based on the solution to the continuous optimization problem. We then compare the asymptotic covariance estimates for LSOI and SIDDS to this lower bound; LSOI is far larger than this lower bound, whereas SIDDS satisfies it almost exactly.

3.1. Covariance Lower Bound. Here we use the constrained variant of the Cramér-Rao lower bound to bound below the covariance of $\bar{\mathbf{c}}$. To begin, let us consider the likelihood function associated with the noise model in (3.1). Suppose our model has estimated the system state sequence $\bar{\mathbf{z}}$ using coefficients $\bar{\mathbf{c}}$ and initial condition \mathbf{z}_1 , the corresponding likelihood is

$$(3.2) \quad p(\bar{\mathbf{y}}; \bar{\mathbf{c}}, \bar{\mathbf{z}}) := \det(2\pi\bar{\Sigma})^{-\frac{1}{2}} \exp[-\frac{1}{2}(\bar{\mathbf{y}} - \bar{\mathbf{z}})^\top \bar{\Sigma}^{-1}(\bar{\mathbf{y}} - \bar{\mathbf{z}})];$$

see, e.g., [29, Sec. 2.2]. This likelihood function does not depend on $\bar{\mathbf{c}}$ explicitly; however $\bar{\mathbf{z}}$ should satisfy the evolution equations, $\mathbf{z}_{j+1} = \mathcal{E}^{\delta j}(\mathbf{z}_1, \mathbf{C})$ (recall \mathcal{E} was defined in (1.18)). We denote this constraint set as

$$(3.3) \quad \Omega := \{\bar{\mathbf{c}}, \bar{\mathbf{z}} : \mathcal{E}^{\delta j}(\mathbf{z}_1, \bar{\mathbf{c}}) = \mathbf{z}_{j+1}, j = 1, \dots, m-1\}.$$

We compute the constrained Cramér-Rao bound following [3] using the Fisher information matrix $\bar{\mathbf{J}}$ and an orthogonal basis for the tangent space of constraints $\bar{\mathbf{U}}(\bar{\mathbf{c}}, \bar{\mathbf{z}})$. For this likelihood function (3.2), the Fisher information matrix is a constant:

$$(3.4) \quad \bar{\mathbf{J}} := \mathbb{E}_{\bar{\mathbf{y}}} \left[\nabla_{\bar{\mathbf{c}}, \bar{\mathbf{z}}}^2 \log p(\bar{\mathbf{y}}; \bar{\mathbf{c}}, \bar{\mathbf{z}}) \right] = \begin{bmatrix} \mathbf{0} & \mathbf{0} \\ \mathbf{0} & \bar{\Sigma}^{-1} \end{bmatrix}$$

where $\mathbb{E}_{\vec{y}}$ denotes the expectation over \vec{y} . Rewriting the constraint set Ω in terms of a function $\vec{g} : \mathbb{R}^{dn} \times \mathbb{R}^{dm} \rightarrow \mathbb{R}^{d(m-1)}$

$$(3.5) \quad \vec{g}(\vec{c}, \vec{z}) := \begin{bmatrix} \mathcal{E}^\delta(\mathbf{z}_1, \vec{c}) - \mathbf{z}_2 \\ \vdots \\ \mathcal{E}^{\delta(m-1)}(\mathbf{z}_1, \vec{c}) - \mathbf{z}_m \end{bmatrix},$$

the tangent space of the constraint $\vec{U}(\vec{c}, \vec{z}) \in \mathbb{R}^{(d(m+n)) \times (d(n+1))}$ satisfies

$$(3.6) \quad \mathbf{0} = [\nabla_{\vec{c}, \vec{z}} \vec{g}(\vec{c}, \vec{z})] \vec{U}(\vec{c}, \vec{z}), \quad \text{and} \quad \vec{U}(\vec{c}, \vec{z})^\top \vec{U}(\vec{c}, \vec{z}) = \mathbf{I}.$$

Let \vec{c}^* and $\vec{z}^* = \vec{x}$ be the true coefficients and states respectively. Then for any estimator that given \vec{y} produces unbiased estimates $\vec{c}^\diamond(\vec{y})$ and $\vec{z}^\diamond(\vec{y})$, namely,

$$(3.7) \quad \mathbb{E}_{\vec{y}} \vec{c}^\diamond(\vec{y}) = \vec{c}^* \quad \text{and} \quad \mathbb{E}_{\vec{y}} \vec{z}^\diamond(\vec{y}) = \vec{z}^* = \vec{x},$$

then \vec{c}^\diamond and \vec{z}^\diamond satisfy the constrained Cramér-Rao lower bound

$$(3.8) \quad \text{Cov}_{\vec{y}} \begin{bmatrix} \vec{c}^\diamond(\vec{y}) \\ \vec{z}^\diamond(\vec{y}) \end{bmatrix} \succeq \vec{U}[\vec{U}^\top \vec{J} \vec{U}]^+ \vec{U}^\top, \quad \vec{U} = \vec{U}(\vec{c}^*, \vec{z}^*),$$

where $\text{Cov}_{\vec{y}}$ denotes the covariance with respect to \vec{y} , $^+$ the pseudoinverse [15, Sec. 5.5.2], and \succeq the ordering of positive semidefinite matrices [19, sec. 7.7].

3.1.1. Covariance of \vec{c} . As our goal is to estimate the coefficients \vec{c} , the estimated state \vec{z} is often a nuisance variable. To compute the covariance of \vec{c} alone, we use the selection matrix $\vec{S}_{\vec{c}} \in \mathbb{R}^{(d(m+n)) \times n_c}$ to pick those columns corresponding to \vec{c} where n_c is the number of entries in \vec{c} ($n_c \neq dn$ when we impose a sparsity constraint). In this case, $\vec{S}_{\vec{c}}$ picks the $(1, 1)$ block:

$$(3.9) \quad \text{Cov } \vec{c}^\diamond \succeq \vec{S}_{\vec{c}}^\top \vec{U}[\vec{U}^\top \vec{J} \vec{U}]^+ \vec{U}^\top \vec{S}_{\vec{c}}.$$

3.1.2. Sparsity Constraint. Imposing a sparsity structure on \vec{c} changes the Cramér-Rao lower bound as this adds an additional constraint. Let $\mathcal{I}(\vec{c})$ select certain indices of \vec{c} ; then the constraint becomes

$$(3.10) \quad \Omega_{\text{sparse}} = \Omega \cap \{\vec{c}, \vec{z} : \mathcal{I}(\vec{c}) = \mathbf{0}\}.$$

Because the constraint set is larger, this decreases the size of the tangent space. This, in general, leads to a smaller covariance of the nonzero entries in the recovered estimate \vec{c}^\diamond .

3.1.3. Computing the Tangent Space. We can compute an orthogonal basis \vec{U} for the tangent space of Ω by solving the sensitivity equations. Let \mathbf{V} be the Jacobian with respect to the coefficients \vec{c} and \mathbf{W} be the Jacobian with respect to the initial conditions

$$(3.11) \quad \mathbf{V}(t) = \nabla_{\vec{c}} \mathcal{E}^t(\mathbf{z}_1, \vec{c}) \in \mathbb{R}^{d \times n_c}, \quad \mathbf{W}(t) = \nabla_{\mathbf{z}_1} \mathcal{E}^t(\mathbf{z}_1, \vec{c}) \in \mathbb{R}^{d \times d}.$$

The vectorized versions of these two quantities, $\vec{v}(t)$ and $\vec{w}(t)$, evolve according to the coupled differential equations

$$(3.12) \quad \begin{cases} \partial_t \mathbf{z}(t) = \mathbf{f}(\mathbf{z}(t), \vec{c}) & \mathbf{z}(0) = \mathbf{z}_0 \\ \partial_t \vec{v}(t) = \mathbf{F}(\mathbf{z}(t), \vec{c}) \vec{v}(t) + \nabla_{\vec{c}} \mathbf{f}(\mathbf{z}(t), \vec{c}) & \vec{v}(0) = \mathbf{0} \\ \partial_t \vec{w}(t) = \mathbf{F}(\mathbf{z}(t), \vec{c}) \vec{w}(t) & \vec{w}(0) = \text{vec}(\mathbf{I}_d) \end{cases}$$

where $\mathbf{F}(\mathbf{z}, \vec{\mathbf{c}}) = \nabla_{\mathbf{z}} \mathbf{f}(\mathbf{z}, \vec{\mathbf{c}}) = \sum_k \mathbf{c}_k \nabla_{\mathbf{z}} \phi_k(\mathbf{z})$. Thus the gradient of $\vec{\mathbf{g}}$ is

$$(3.13) \quad \nabla_{\vec{\mathbf{c}}, \vec{\mathbf{z}}} \vec{\mathbf{g}}(\vec{\mathbf{c}}, \vec{\mathbf{z}}) = \nabla_{\vec{\mathbf{c}}, \vec{\mathbf{z}}} \begin{bmatrix} \mathcal{E}^\delta(\mathbf{z}_1, \vec{\mathbf{c}}) - \mathbf{z}_2 \\ \mathcal{E}^{2\delta}(\mathbf{z}_1, \vec{\mathbf{c}}) - \mathbf{z}_3 \\ \vdots \\ \mathcal{E}^{m\delta}(\mathbf{z}_1, \vec{\mathbf{c}}) - \mathbf{z}_m \end{bmatrix} = \begin{bmatrix} \mathbf{V}(\delta) & \mathbf{W}(\delta) & -\mathbf{I} & & \\ \mathbf{V}(2\delta) & \mathbf{W}(2\delta) & & -\mathbf{I} & \\ \vdots & \vdots & & & \ddots \\ \mathbf{V}(m\delta) & \mathbf{W}(m\delta) & & & -\mathbf{I} \end{bmatrix}.$$

The structure in this matrix allows us to write down an explicit formula its nullspace,

$$(3.14) \quad \text{Null } \nabla_{\vec{\mathbf{c}}, \vec{\mathbf{z}}} \vec{\mathbf{g}}(\vec{\mathbf{c}}, \vec{\mathbf{z}}) = \text{Range} \left(\begin{bmatrix} \mathbf{I} & \mathbf{0} \\ \mathbf{0} & \mathbf{I} \\ \mathbf{V}(\delta) & \mathbf{W}(\delta) \\ \vdots & \vdots \\ \mathbf{V}(m\delta) & \mathbf{W}(m\delta) \end{bmatrix} \right).$$

Thus we can compute an orthogonal basis for the tangent space of Ω at $\vec{\mathbf{c}}, \vec{\mathbf{z}}$, namely, $\vec{\mathbf{U}}(\vec{\mathbf{c}}, \vec{\mathbf{z}})$, by performing a reduced QR-factorization of this matrix above.

3.2. Performance of LSOI. Let $\vec{\mathbf{c}}^\star = \vec{\mathbf{c}}^\star(\vec{\mathbf{y}})$ be the coefficient estimate provided by LSOI (1.9),

$$(3.15) \quad \vec{\mathbf{c}}^\star := \underset{\vec{\mathbf{c}}}{\text{argmin}} \|\vec{\mathbf{D}}\vec{\mathbf{y}} - \vec{\Phi}(\vec{\mathbf{y}})\vec{\mathbf{c}}\|_2^2.$$

We can alternatively write this solution using the pseudoinverse $^+$,

$$(3.16) \quad \vec{\mathbf{c}}^\star = \vec{\Phi}^+(\vec{\mathbf{y}})\vec{\mathbf{D}}\vec{\mathbf{y}}.$$

Assuming $\vec{\mathbf{y}} = \vec{\mathbf{x}} + \sigma \vec{\mathbf{n}}$ with $\vec{\mathbf{n}} \sim \mathcal{N}(\mathbf{0}, \Sigma)$, in the limit of small noise ($\sigma \rightarrow 0$),

$$(3.17) \quad \vec{\mathbf{c}}^\star = \vec{\Phi}^+(\vec{\mathbf{x}} + \sigma \vec{\mathbf{n}})\vec{\mathbf{D}}(\vec{\mathbf{x}} + \sigma \vec{\mathbf{n}})$$

$$(3.18) \quad = \vec{\Phi}^+(\vec{\mathbf{x}})\vec{\mathbf{D}}\vec{\mathbf{x}} + \sigma \left([\nabla \vec{\Phi}^+(\vec{\mathbf{x}})] \bar{\mathbf{x}}_3 \vec{\mathbf{n}} \right) \vec{\mathbf{D}}\vec{\mathbf{x}} + \sigma \vec{\Phi}^+(\vec{\mathbf{x}})\vec{\mathbf{D}}\vec{\mathbf{n}} + \mathcal{O}(\sigma^2)$$

$$(3.19) \quad = \vec{\Phi}^+(\vec{\mathbf{x}})\vec{\mathbf{D}}\vec{\mathbf{x}} + \sigma \left([\nabla \vec{\Phi}^+(\vec{\mathbf{x}})] \bar{\mathbf{x}}_2 (\vec{\mathbf{D}}\vec{\mathbf{x}}) + \vec{\Phi}^+(\vec{\mathbf{x}})\vec{\mathbf{D}} \right) \vec{\mathbf{n}} + \mathcal{O}(\sigma^2).$$

Let this first order transformation of $\vec{\mathbf{n}}$ be denoted by

$$(3.20) \quad \vec{\mathbf{T}}_\bullet := [\nabla \vec{\Phi}^+(\vec{\mathbf{x}})] \bar{\mathbf{x}}_2 (\vec{\mathbf{D}}\vec{\mathbf{x}}) + \vec{\Phi}^+(\vec{\mathbf{x}})\vec{\mathbf{D}}.$$

To first order, $\vec{\mathbf{c}}^\star$ has a bias proportional to finite difference error in the derivative,

$$(3.21) \quad \mathbb{E}[\vec{\mathbf{c}}^\star - \vec{\mathbf{c}}^\star] = \vec{\Phi}^+(\vec{\mathbf{x}})\vec{\mathbf{D}}\vec{\mathbf{x}} - \vec{\mathbf{c}}^\star + \mathbb{E}_{\vec{\mathbf{n}}}[\vec{\mathbf{T}}_\bullet \vec{\mathbf{n}}] + \mathcal{O}(\sigma^2)$$

$$(3.22) \quad = \vec{\Phi}^+(\vec{\mathbf{x}})(\vec{\mathbf{D}}\vec{\mathbf{x}} - \vec{\mathbf{x}}) + \mathcal{O}(\sigma^2),$$

since $\dot{\vec{\mathbf{x}}} = \vec{\Phi}(\vec{\mathbf{x}})\vec{\mathbf{c}}^\star$ where $\dot{\vec{\mathbf{x}}}$ denotes the state derivative. Similarly, the covariance is

$$(3.23) \quad \text{Cov } \vec{\mathbf{c}}^\star = \sigma^2 \vec{\mathbf{T}}_\bullet \bar{\Sigma} \vec{\mathbf{T}}_\bullet^\top + \mathcal{O}(\sigma^3).$$

We can explicitly compute $\vec{\mathbf{T}}_\bullet$ by using Golub and Pereyra's formula for the derivative of a pseudoinverse [14, eq. (4.12)]; denoting by ∂_i the derivative of the i th entry of $\vec{\mathbf{c}}$ and omitting arguments,

$$(3.24) \quad \partial_i \vec{\Phi}^+ = -\vec{\Phi}^+ [\partial_i \vec{\Phi}] \vec{\Phi}^+ + \vec{\Phi}^+ \vec{\Phi}^{+\top} [\partial_i \vec{\Phi}^\top] (\mathbf{I} - \vec{\Phi} \vec{\Phi}^+) + (\mathbf{I} - \vec{\Phi}^+ \vec{\Phi}) [\partial_i \vec{\Phi}^\top] \vec{\Phi}^+ \vec{\Phi}^+.$$

Next, using this asymptotic analysis, we demonstrate LSOI yields suboptimal estimates. In the following examples, we consider the simple harmonic oscillator example from the introduction with a fixed sparsity pattern selecting the true, nonzero values of $\vec{\mathbf{c}}$. Taking $\vec{\mathbf{n}} \sim \mathcal{N}(\vec{\mathbf{0}}, \sigma^2 \mathbf{I})$ with $\sigma = 10^{-2}$, we compute a Monte Carlo estimate of the covariance of $\vec{\mathbf{c}}^\star$, the asymptotic estimate (3.23), and the Cramér-Rao lower bound (3.9)

Monte Carlo Cov[$\vec{\mathbf{c}}^\star$]	Asymptotic Cov[$\vec{\mathbf{c}}^\star$]	Unbiased CRLB
$\sigma^2 \begin{bmatrix} 0.058709 & 0.001283 \\ 0.001283 & 0.076960 \end{bmatrix}$	$\sigma^2 \begin{bmatrix} 0.057869 & 0.002001 \\ 0.002001 & 0.075413 \end{bmatrix}$	$\sigma^2 \begin{bmatrix} 0.002015 & 0.001990 \\ 0.001990 & 0.002024 \end{bmatrix}$

This example shows that both asymptotic estimate provides an accurate covariance and the covariance LSOI is substantially larger than the lower bound. In this previous example, we used a 3-point finite difference rule. We might expect that using a higher order finite difference approximation would decrease the covariance; in fact, the opposite happens! Considering the asymptotic covariance for the same problem, we observe

3-point rule Cov[$\vec{\mathbf{c}}^\star$]	5-point rule Cov[$\vec{\mathbf{c}}^\star$]	7-point rule Cov[$\vec{\mathbf{c}}^\star$]
$\sigma^2 \begin{bmatrix} 0.057869 & 0.002001 \\ 0.002001 & 0.075413 \end{bmatrix}$	$\sigma^2 \begin{bmatrix} 0.147962 & 0.002001 \\ 0.002001 & 0.193098 \end{bmatrix}$	$\sigma^2 \begin{bmatrix} 0.943824 & 0.002001 \\ 0.002001 & 1.240532 \end{bmatrix}$

The exact origin of this effect is unclear, but it is likely a result of the increased bandwidth of $\vec{\mathbf{D}}$. This result provides yet another reason that high order differencing schemes are not frequently seen in other work.

3.3. Performance of SIDDS. Here we consider the SIDDS problem with a weighted objective that maximizes the likelihood of $\vec{\mathbf{z}}$

$$(3.25) \quad \begin{aligned} \vec{\mathbf{c}}^\star, \vec{\mathbf{z}}^\star = & \underset{\vec{\mathbf{c}} \in \mathbb{R}^{dn}, \vec{\mathbf{z}} \in \mathbb{R}^{dm}}{\operatorname{argmin}} \quad \frac{1}{2} (\vec{\mathbf{y}} - \vec{\mathbf{z}})^\top \vec{\Sigma}^{-1} (\vec{\mathbf{y}} - \vec{\mathbf{z}}) \\ & \text{s.t. } \vec{\mathbf{D}} \vec{\mathbf{z}} = \vec{\Phi}(\vec{\mathbf{z}}) \vec{\mathbf{c}}. \end{aligned}$$

As before, we consider the limit of small noise $\vec{\mathbf{y}} = \vec{\mathbf{x}} + \sigma \vec{\mathbf{n}}$ with $\sigma \rightarrow 0$ and construct perturbation estimates around the true values

$$(3.26) \quad \vec{\mathbf{c}}^\star = \vec{\mathbf{c}}^\star + \sigma \vec{\mathbf{c}}^{(1)} + \mathcal{O}(\sigma^2) \quad \vec{\mathbf{z}}^\star = \vec{\mathbf{z}} + \sigma \vec{\mathbf{z}}^{(1)} + \mathcal{O}(\sigma^2).$$

Linearizing the constraint of (3.25) around the zeroth order terms yields the quadratic program with Karush-Kuhn-Tucker (KKT) system

$$(3.27) \quad \begin{bmatrix} \mathbf{0} & \sigma^2 \vec{\Sigma}^{-1} & \vec{\mathbf{K}}^\top \\ \vec{\mathbf{K}} & \vec{\mathbf{L}} & \mathbf{0} \end{bmatrix} \begin{bmatrix} \vec{\mathbf{c}}^{(1)} \\ \vec{\mathbf{z}}^{(1)} \\ \vec{\mathbf{w}} \end{bmatrix} = \begin{bmatrix} \vec{\mathbf{0}} \\ \sigma^2 \vec{\Sigma}^{-1} \vec{\mathbf{n}} \\ -\vec{\mathbf{h}}(\vec{\mathbf{c}}, \vec{\mathbf{x}}) \end{bmatrix}$$

where $\vec{\mathbf{h}}$ is the constraint defined in (2.6) and $\vec{\mathbf{K}}$ and $\vec{\mathbf{L}}$ are the two blocks in the constraint derivative (2.7). To compute $\vec{\mathbf{c}}^{(1)}$ and $\vec{\mathbf{z}}^{(1)}$ we used a reduced Hessian approach where $\vec{\mathbf{U}}_\bullet$ is an orthogonal basis for the nullspace of $[\vec{\mathbf{K}} \quad \vec{\mathbf{L}}]$,

$$(3.28) \quad \begin{bmatrix} \vec{\mathbf{c}}^{(1)} \\ \vec{\mathbf{z}}^{(1)} \end{bmatrix} = -[\vec{\mathbf{K}} \quad \vec{\mathbf{L}}]^+ \vec{\mathbf{h}}(\vec{\mathbf{c}}^\star, \vec{\mathbf{x}}) + \vec{\mathbf{U}}_\bullet \left(\vec{\mathbf{U}}_\bullet^\top \begin{bmatrix} \mathbf{0} & \vec{\Sigma}^{-1} \end{bmatrix} \vec{\mathbf{U}}_\bullet \right)^+ \vec{\mathbf{U}}_\bullet^\top \begin{bmatrix} \vec{\mathbf{0}} \\ \vec{\Sigma}^{-1} \vec{\mathbf{n}} \end{bmatrix}.$$

As with LSOI, we note that SIDDS has a slight bias since the discretized constraint $\vec{\mathbf{h}}(\vec{\mathbf{c}}^*, \vec{\mathbf{x}})$ is not necessarily satisfied exactly

$$(3.29) \quad \mathbb{E} \begin{bmatrix} \vec{\mathbf{c}}^\bullet - \vec{\mathbf{c}}^* \\ \vec{\mathbf{z}}^\bullet - \vec{\mathbf{x}} \end{bmatrix} = - [\vec{\mathbf{K}} \quad \vec{\mathbf{L}}]^+ \vec{\mathbf{h}}(\vec{\mathbf{c}}^*, \vec{\mathbf{x}}) + \mathcal{O}(\sigma^2).$$

Using a higher order finite difference scheme makes this bias small; returning to the simple harmonic oscillator example with fixed sparsity and $\vec{\mathbf{n}} \sim \mathcal{N}(\vec{\mathbf{0}}, \vec{\mathbf{I}})$

$$\begin{array}{ccc} \text{3-point } \mathbb{E}[\vec{\mathbf{c}}^\bullet - \vec{\mathbf{c}}^*] & \text{5-point } \mathbb{E}[\vec{\mathbf{c}}^\bullet - \vec{\mathbf{c}}^*] & \text{7-point } \mathbb{E}[\vec{\mathbf{c}}^\bullet - \vec{\mathbf{c}}^*] \\ \begin{bmatrix} -0.057191 \\ 0.109035 \end{bmatrix} & \begin{bmatrix} -1.569746 \cdot 10^{-7} \\ 1.417364 \cdot 10^{-7} \end{bmatrix} & \begin{bmatrix} -1.566412 \cdot 10^{-7} \\ 1.414032 \cdot 10^{-7} \end{bmatrix} \end{array}.$$

Note that this bias almost exactly matches the error in the example in subsection 1.5.

The covariance of SIDDS has an identical form to the Cramér-Rao lower bound,

$$(3.30) \quad \text{Cov } \vec{\mathbf{c}}^\bullet = \vec{\mathbf{S}}_c^\top \vec{\mathbf{U}}_\bullet (\vec{\mathbf{U}}_\bullet^\top \vec{\mathbf{J}} \vec{\mathbf{U}}_\bullet)^+ \vec{\mathbf{U}}_\bullet^\top \vec{\mathbf{S}}_c$$

where tangent space for the continuous constraint $\vec{\mathbf{U}}$ has been replaced with the tangent space for the discretized constraint $\vec{\mathbf{U}}_\bullet$. Typically, the subspace angle between these two spaces is small leading $\vec{\mathbf{c}}^\bullet$ to nearly obtain the lower bound:

$$\begin{array}{ccc} \text{3-point Cov } \vec{\mathbf{c}}^\bullet & \text{5-point Cov } \vec{\mathbf{c}}^\bullet & \text{Unbiased CRLB} \\ \begin{bmatrix} 0.002007 & 0.001995 \\ 0.001995 & 0.002004 \end{bmatrix} & \begin{bmatrix} 0.002015 & 0.001990 \\ 0.001990 & 0.002024 \end{bmatrix} & \begin{bmatrix} 0.002015 & 0.001990 \\ 0.001990 & 0.002024 \end{bmatrix} \end{array}.$$

Unlike LSOI, higher order difference schemes for SIDDS yield better estimates. Note the 3-point covariance is slightly smaller than the unbiased Cramér-Rao lower bound which is possible due to its bias; the 5-point covariance matches the lower bound with an error around 10^{-7} .

4. Solving SIDDS. The following two sections discuss how we solve both SIDDS and sparsity promoting variant using a weighted ℓ_2 -norm objective:

$$(4.1) \quad \begin{array}{ll} \min_{\vec{\mathbf{c}}, \vec{\mathbf{z}}} (\vec{\mathbf{y}} - \vec{\mathbf{z}})^\top \vec{\mathbf{M}} (\vec{\mathbf{y}} - \vec{\mathbf{z}}) + \alpha R_p(\vec{\mathbf{c}}) & \text{recall } R_p(\vec{\mathbf{c}}) := \begin{cases} \|\vec{\mathbf{c}}\|_p^p, & p > 0; \\ \|\vec{\mathbf{c}}\|_0, & p = 0; \end{cases} \\ \text{s.t. } \vec{\mathbf{D}}_p \vec{\mathbf{z}} = \vec{\Phi}(\vec{\mathbf{z}}) \vec{\mathbf{c}}; \end{array}$$

and $\vec{\mathbf{M}} \in \mathbb{R}^{(dm) \times (dm)}$ is positive semidefinite. In this section we discuss initialization and how we approximate R_p using IRLS yielding a quadratic objective. Then, in the next section, we show how to efficiently solve this optimization problem.

4.1. Initialization. Since (4.1) is a nonconvex optimization problem, we are not guaranteed convergence to a global optimum from arbitrary initial estimates. Hence our choice to initialize $\vec{\mathbf{c}}$ and $\vec{\mathbf{z}}$ are important to ensure convergence to a good local minimizer. In many experiments, simply taking $\vec{\mathbf{z}}^{(0)} = \vec{\mathbf{y}}$ and $\vec{\mathbf{c}}^{(0)} = \mathbf{0}$ is sufficient (henceforth superscripts denote iteration number). However with large noise, we find better minimizers by applying modest amount of smoothing. Here we use Tikhonov smoothing to estimate $\vec{\mathbf{z}}^{(0)}$

$$(4.2) \quad \vec{\mathbf{z}}^{(0)} = \underset{\vec{\mathbf{z}}}{\text{argmin}} \left\| \begin{bmatrix} \vec{\mathbf{y}} \\ \mathbf{0} \end{bmatrix} - \begin{bmatrix} \mathbf{I} \\ \lambda \vec{\mathbf{D}}^2 \end{bmatrix} \vec{\mathbf{z}} \right\|_2^2$$

where $\lambda > 0$ is a smoothing parameter (in our experiments $\lambda = 10^{-2}$) and $\vec{\mathbf{D}}^2$ is a 3-point finite-difference approximation of the second derivative. Then we apply LSOI to estimate $\vec{\mathbf{c}}^{(0)}$ based on $\vec{\mathbf{z}}^{(0)}$. We expect more sophisticated initialization strategies, e.g., those in [10], could yield further improvements but leave this to future work.

Algorithm 4.1 SIDDS with IRLS Regularization Approximation

Input : measurements \vec{y} , regularization order p , regularization weight α
Output : denoised state \vec{z} , parameter estimates \vec{c}

- 1 Initialize $\epsilon^{(0)} \leftarrow 1$, $\vec{z}^{(0)}$ by smoothing (4.2), $\vec{c}^{(0)}$ by LSOI (1.9) applied to $\vec{z}^{(0)}$;
- 2 **for** $\ell = 1, 2, 3, \dots$ **do**
- 3 $\vec{W}^{(\ell-1)} \leftarrow \text{diag}(|\vec{c}^{(\ell-1)}|^2 + \epsilon^{(\ell-1)})^{\frac{p}{2}-1}$;
- 4 Obtain $\vec{c}^{(\ell)}$ and $\vec{z}^{(\ell)}$ by one step of SQP applied to
 $\min_{\vec{c}, \vec{z}} (\vec{y} - \vec{z})^\top \vec{M}(\vec{y} - \vec{z}) + \alpha \vec{c}^\top \vec{W}^{(\ell-1)} \vec{c} \quad \text{s.t.} \quad \vec{D}\vec{z} = \vec{\Phi}(\vec{z})\vec{c}$;
- 5 **if** *optimization converged* **then** $\epsilon^{(\ell)} \leftarrow \epsilon^{(\ell-1)}/10$;
- 6 **else** $\epsilon^{(\ell)} \leftarrow \epsilon^{(\ell-1)}$;
- 7 **if** *optimization converged and* $\epsilon^{(\ell)} < 10^{-8}$ **then break**;

4.2. Approximating Regularization via IRLS. The regularization R_p in the objective (4.1) presents a challenge. For $p \geq 1$, R_p is convex, but concave for $p < 1$. However it is when $p < 1$, and in particular $p = 0$, that this regularization will most effectively promote sparsity. One approach would be to simply apply SQP directly to (4.1) but this would introduce negative curvature in the Hessian. Instead, we replace R_p with an IRLS approximation [4, subsec. 4.5.2] producing a positive definite Hessian. At the ℓ th iterate, the IRLS approximation is

$$(4.3) \quad R_p(\vec{c}^{(\ell)}) := \sum_i |c_i^{(\ell)}|^p = \sum_i |c_i^{(\ell)}|^{p-2} |c_i^{(\ell)}|^2 \approx \sum_i |c_i^{(\ell-1)}|^{p-2} |c_i^{(\ell)}|^2.$$

If $\vec{c}^{(\ell-1)} \rightarrow \vec{c}^{(\ell)}$ as $\ell \rightarrow \infty$, this IRLS approximation approaches R_p . Numerically, when $c_i^{(\ell-1)}$ is small and $p < 2$, we can encounter a divide by zero error. We avoid this by following Chartrand and Yin [8] and add a small iteration dependent regularization $\epsilon^{(\ell)} > 0$. This yields the quadratic approximation:

$$(4.4) \quad R_p(\vec{c}) \approx R_p^{(\ell)}(\vec{c}) := \vec{c}^\top \vec{W}^{(\ell-1)} \vec{c}, \quad \vec{W}^{(\ell)} := \text{diag} \left(\left\{ [|c_i^{(\ell)}|^2 + \epsilon^{(\ell)}]^{\frac{p}{2}-1} \right\}_i \right).$$

As the optimization proceeds, we let $\epsilon^{(\ell)} \rightarrow 0$. We opt for the simple heuristic of decreasing ϵ by a factor of ten when optimization terminates successfully following [8], although more sophisticated heuristics exist [11, 25].

We summarize the initialization, regularization approximation, and IRLS update in Algorithm 4.1; the next section shows how to efficiently perform the SQP step.

5. Solution of the Optimization Problem. Having introduced the IRLS relaxation of the ℓ_p -norm constraint, we now seek to solve the corresponding optimization problem. At each step we solve

$$(5.1) \quad \begin{aligned} \min_{\vec{c}, \vec{z}} f(\vec{c}, \vec{z}) &:= \frac{1}{2} (\vec{y} - \vec{z})^\top \vec{M}(\vec{y} - \vec{z}) + \frac{\alpha}{2} \vec{c}^\top \vec{W} \vec{c} \\ \text{s.t. } \vec{h}(\vec{c}, \vec{z}) &:= \vec{D}\vec{z} - \vec{\Phi}(\vec{z})\vec{c} = \mathbf{0} \end{aligned}$$

We use a SQP approach since this problem is nearly a quadratic program (and would be if $\vec{\Phi}(\vec{z})$ was constant). Here we use the SQP approach of Liu and Yuan [26] to ensure convergence of the SQP iterates without the use of a merit function or filter. Each step requires the solution of two large-scale subproblems. In this section, we

show how both can be efficiently solved by exploiting the structure of this optimization problem. We conclude by showing how these same techniques can be used with multiple trajectories.

5.1. Relaxation Step. The relaxation step seeks to find a direction $\vec{\mathbf{p}}^{(\ell)}$ that approximately minimizes the error in the linearization of the constraints:

$$(5.2) \quad \vec{\mathbf{p}}^{(\ell)} \approx \underset{\vec{\mathbf{p}}}{\operatorname{argmin}} \|\vec{\mathbf{h}}^{(\ell)} + \vec{\mathbf{A}}^{(\ell)} \vec{\mathbf{p}}\|_2^2,$$

$$(5.3) \quad \text{where } \vec{\mathbf{A}}^{(\ell)} := \vec{\mathbf{A}}(\vec{\mathbf{c}}^{(\ell)}, \vec{\mathbf{z}}^{(\ell)}) \quad \vec{\mathbf{A}}(\vec{\mathbf{c}}, \vec{\mathbf{z}}) := [\nabla_{\vec{\mathbf{c}}} \vec{\mathbf{h}}(\vec{\mathbf{c}}, \vec{\mathbf{z}}) \quad \nabla_{\vec{\mathbf{z}}} \vec{\mathbf{h}}(\vec{\mathbf{c}}, \vec{\mathbf{z}})],$$

and $\vec{\mathbf{h}}^{(\ell)} := \vec{\mathbf{h}}(\vec{\mathbf{c}}^{(\ell)}, \vec{\mathbf{z}}^{(\ell)})$. For the convergence analysis of [26] to hold, this direction $\vec{\mathbf{p}}^{(\ell)}$ must satisfy two constraints for small constants κ_1 and κ_2

$$(5.4) \quad \|\vec{\mathbf{p}}^{(\ell)}\| \leq \kappa_1 \|\vec{\mathbf{A}}^{(\ell)\top} \vec{\mathbf{h}}^{(\ell)}\|, \quad \kappa_1 \geq 0;$$

$$(5.5) \quad \|\vec{\mathbf{h}}^{(\ell)}\|^2 - \|\vec{\mathbf{h}}^{(\ell)}\| \|\vec{\mathbf{h}}^{(\ell)} + \vec{\mathbf{A}}^{(\ell)} \vec{\mathbf{p}}^{(\ell)}\| \geq \kappa_2 \|\vec{\mathbf{A}}^{(\ell)\top} \vec{\mathbf{h}}^{(\ell)}\|^2, \quad \kappa_2 \in (0, 1).$$

Due to the scale of $\vec{\mathbf{A}} \in \mathbb{R}^{(dn) \times (dm+dn)}$, direct solution methods for (5.2) are impractical. Instead, we compute the relaxation step by exploiting the structure of $\vec{\mathbf{A}}^{(\ell)}$. The matrix $\vec{\mathbf{A}}^{(\ell)}$ contains two blocks $\vec{\mathbf{A}}^{(\ell)} = [\vec{\mathbf{K}}^{(\ell)} \quad \vec{\mathbf{L}}^{(\ell)}]$ where

$$(5.6) \quad \vec{\mathbf{K}}^{(\ell)} := \vec{\mathbf{K}}(\vec{\mathbf{c}}^{(\ell)}, \vec{\mathbf{z}}^{(\ell)}); \quad \vec{\mathbf{K}}(\vec{\mathbf{c}}, \vec{\mathbf{z}}) := \nabla_{\vec{\mathbf{c}}} \vec{\mathbf{h}}(\vec{\mathbf{c}}, \vec{\mathbf{z}}) = -\vec{\Phi}(\vec{\mathbf{z}});$$

$$(5.7) \quad \vec{\mathbf{L}}^{(\ell)} := \vec{\mathbf{L}}(\vec{\mathbf{c}}^{(\ell)}, \vec{\mathbf{z}}^{(\ell)}); \quad \vec{\mathbf{L}}(\vec{\mathbf{c}}, \vec{\mathbf{z}}) := \nabla_{\vec{\mathbf{z}}} \vec{\mathbf{h}}(\vec{\mathbf{c}}, \vec{\mathbf{z}}) = \vec{\mathbf{D}} - \nabla \vec{\Phi}(\vec{\mathbf{z}}) \bar{\times}_2 \vec{\mathbf{c}}.$$

Our approach is to split $\vec{\mathbf{p}}$ into components corresponding to $\vec{\mathbf{c}}$ and $\vec{\mathbf{z}}$:

$$(5.8) \quad \|\vec{\mathbf{h}}^{(\ell)} + \vec{\mathbf{A}}^{(\ell)} \vec{\mathbf{p}}\|_2^2 = \|\vec{\mathbf{h}}^{(\ell)} + \vec{\mathbf{K}}^{(\ell)} \vec{\mathbf{p}}_{\vec{\mathbf{c}}} + \vec{\mathbf{L}}^{(\ell)} \vec{\mathbf{p}}_{\vec{\mathbf{z}}}\|_2^2 \quad \text{where } \vec{\mathbf{p}} = \begin{bmatrix} \vec{\mathbf{p}}_{\vec{\mathbf{c}}} \\ \vec{\mathbf{p}}_{\vec{\mathbf{z}}} \end{bmatrix}$$

and then solve for $\vec{\mathbf{p}}_{\vec{\mathbf{c}}}$ and $\vec{\mathbf{p}}_{\vec{\mathbf{z}}}$ separately.

We compute $\vec{\mathbf{p}}_{\vec{\mathbf{c}}}^{(\ell)}$ by setting $\vec{\mathbf{p}}_{\vec{\mathbf{z}}} = \mathbf{0}$ and solving the overdetermined least squares problem

$$(5.9) \quad \vec{\mathbf{p}}_{\vec{\mathbf{c}}}^{(\ell)} := \underset{\vec{\mathbf{p}}_{\vec{\mathbf{c}}}}{\operatorname{argmin}} \|\vec{\mathbf{h}}^{(\ell)} + \vec{\mathbf{K}}^{(\ell)} \vec{\mathbf{p}}_{\vec{\mathbf{c}}}\|_2^2$$

$$(5.10) \quad = \underset{\vec{\mathbf{p}}_{\vec{\mathbf{c}}}}{\operatorname{argmin}} \|\vec{\Phi}(\vec{\mathbf{z}}^{(\ell)}) \vec{\mathbf{p}}_{\vec{\mathbf{c}}} - [\vec{\mathbf{D}} \vec{\mathbf{z}}^{(\ell)} - \vec{\Phi}(\vec{\mathbf{z}}^{(\ell)}) \vec{\mathbf{c}}^{(\ell)}]\|_2^2.$$

This second statement has the same structure as LSOI (1.9) allowing us to restate this in a dense matrix format, removing the Kronecker products:

$$(5.11) \quad \mathbf{P}_{\mathbf{C}}^{(\ell)} := \underset{\mathbf{P}_{\mathbf{C}}}{\operatorname{argmin}} \|\Phi(\mathbf{Z}^{(\ell)}) \mathbf{P}_{\mathbf{C}} - [\mathbf{DZ}^{(\ell)} - \Phi(\mathbf{Z}^{(\ell)}) \mathbf{C}^{(\ell)}]\|_{\mathbf{F}}^2.$$

This allows more efficient solution via a QR factorization and we set $\vec{\mathbf{p}}_{\vec{\mathbf{c}}}^{(\ell)} = \operatorname{vec}(\mathbf{P}_{\mathbf{C}}^{(\ell)})$.

Next, we solve for $\vec{\mathbf{p}}_{\vec{\mathbf{z}}}$ holding $\vec{\mathbf{p}}_{\vec{\mathbf{c}}}$ constant:

$$(5.12) \quad \vec{\mathbf{p}}_{\vec{\mathbf{z}}}^{(\ell)} \approx \underset{\vec{\mathbf{p}}_{\vec{\mathbf{z}}}}{\operatorname{argmin}} \|\vec{\mathbf{h}}^{(\ell)} + \vec{\mathbf{K}}^{(\ell)} \vec{\mathbf{p}}_{\vec{\mathbf{c}}}^{(\ell)} + \vec{\mathbf{L}}^{(\ell)} \vec{\mathbf{p}}_{\vec{\mathbf{z}}}\|_2^2.$$

Although $\vec{\mathbf{L}}^{(\ell)}$ is square, it is structurally rank deficient. The matrix $\vec{\mathbf{L}}^{(\ell)}$ encodes the discretized constraint for $\mathcal{E}^{\delta(j-1)}(\mathbf{z}_1, \vec{\mathbf{c}}) = \mathbf{z}_j$ for $j = 2, \dots, m$; this continuous

constraint only provides $d(m-1)$ constraints whereas $\vec{\mathbf{L}}^{(\ell)}$ encodes dm constraints. Thus when approximating $\vec{\mathbf{p}}_{\vec{\mathbf{z}}}$ we include a small amount of Tikhonov regularization and solve via the normal equations:

$$(5.13) \quad \vec{\mathbf{p}}_{\vec{\mathbf{z}}}^{(\ell)} := -[\vec{\mathbf{L}}^{(\ell)\top} \vec{\mathbf{L}}^{(\ell)} + \beta \mathbf{I}]^{-1} \vec{\mathbf{L}}^{(\ell)\top} [\vec{\mathbf{h}}^{(\ell)} + \vec{\mathbf{K}}^{(\ell)} \vec{\mathbf{p}}_{\vec{\mathbf{c}}}^{(\ell)}];$$

in our numerical experiments we take $\beta = 10^{-6}$. Since $\vec{\mathbf{L}}^{(\ell)} \in \mathbb{R}^{(dm) \times (dm)}$ has small bandwidth $dq \ll dm$, we apply the inverse using a sparse LU factorization.

5.2. Solution of Quadratic Subproblem. The other expensive component of the Liu and Yuan SQP algorithm is solving the relaxed quadratic program

$$(5.14) \quad \begin{aligned} \vec{\mathbf{d}}^{(\ell)} = \underset{\vec{\mathbf{d}}}{\operatorname{argmin}} \quad & \vec{\mathbf{g}}^{(\ell)\top} \vec{\mathbf{d}} + \frac{1}{2} \vec{\mathbf{d}}^\top \vec{\mathbf{B}}^{(\ell)} \vec{\mathbf{d}} \\ \text{s.t.} \quad & \vec{\mathbf{A}}^{(\ell)} \vec{\mathbf{d}} = \vec{\mathbf{A}}^{(\ell)} \vec{\mathbf{p}}^{(\ell)} \end{aligned}$$

where $\vec{\mathbf{B}}^{(\ell)}$ is an approximation of the Lagrangian Hessian and $\vec{\mathbf{g}}^{(\ell)}$ is the gradient

$$(5.15) \quad \vec{\mathbf{g}}^{(\ell)} := \vec{\mathbf{g}}(\vec{\mathbf{c}}^{(\ell)}, \vec{\mathbf{z}}^{(\ell)}) \quad \vec{\mathbf{g}}(\vec{\mathbf{c}}, \vec{\mathbf{z}}) := [\nabla_{\vec{\mathbf{c}}} f(\vec{\mathbf{c}}, \vec{\mathbf{z}}) \quad \nabla_{\vec{\mathbf{z}}} f(\vec{\mathbf{c}}, \vec{\mathbf{z}})].$$

Here we introduce a sparse approximation of the $\vec{\mathbf{B}}^{(\ell)}$ and show how to efficiently solve (5.14) by direct solution of the stabilized KKT system with a preconditioned MINRES iteration.

Ideally we would use the exact Hessian of the Lagrangian for $\vec{\mathbf{B}}^{(\ell)}$

$$(5.16) \quad \mathcal{L}(\vec{\mathbf{c}}, \vec{\mathbf{z}}, \vec{\mathbf{w}}) := f(\vec{\mathbf{c}}, \vec{\mathbf{z}}) + \vec{\mathbf{w}}^\top \vec{\mathbf{h}}(\vec{\mathbf{c}}, \vec{\mathbf{z}}),$$

where $\vec{\mathbf{w}}$ are the Lagrange multipliers. However, this choice is impractical as $\nabla_{\vec{\mathbf{c}}, \vec{\mathbf{z}}}^2 \mathcal{L}$ will generally be dense. Note the contribution from the Lagrange multiplier term is

$$(5.17) \quad \vec{\mathbf{w}}^\top \vec{\mathbf{h}}(\vec{\mathbf{c}}, \vec{\mathbf{z}}) = \vec{\mathbf{w}}^\top \vec{\mathbf{D}}_p \vec{\mathbf{z}} - \vec{\mathbf{w}}^\top \vec{\Phi}(\vec{\mathbf{z}}) \vec{\mathbf{c}};$$

the Hessian of this second term $\vec{\mathbf{w}}^\top \vec{\Phi}(\vec{\mathbf{z}}) \vec{\mathbf{c}}$ will be dense except for special combinations of $\vec{\mathbf{c}}$ and basis vectors ϕ_k . Instead we will neglect the contribution from this term entirely, and approximate the Lagrangian Hessian by the Hessian of the objective:

$$(5.18) \quad \vec{\mathbf{B}}^{(\ell)} := \nabla_{\vec{\mathbf{c}}, \vec{\mathbf{z}}}^2 f(\vec{\mathbf{c}}^{(\ell)}, \vec{\mathbf{z}}^{(\ell)}) = \begin{bmatrix} \alpha \vec{\mathbf{W}}^{(\ell)} & \mathbf{0} \\ \mathbf{0} & \vec{\mathbf{M}} \end{bmatrix};$$

by construction, this is a positive semidefinite matrix.

Next, we seek to solve the KKT system

$$(5.19) \quad \begin{bmatrix} \vec{\mathbf{B}}^{(\ell)} & \vec{\mathbf{A}}^{(\ell)\top} \\ \vec{\mathbf{A}}^{(\ell)} & \mathbf{0} \end{bmatrix} \begin{bmatrix} \vec{\mathbf{d}} \\ \vec{\mathbf{w}} \end{bmatrix} = \begin{bmatrix} -\vec{\mathbf{g}}^{(\ell)} \\ \vec{\mathbf{A}}^{(\ell)} \vec{\mathbf{p}}^{(\ell)} \end{bmatrix}.$$

Since $\vec{\mathbf{L}}^{(\ell)}$ is rank deficient, $\vec{\mathbf{A}}^{(\ell)}$ does not have full row rank causing the KKT system to be singular. To correct this, we use a stabilization procedure following Wright [32, eq. (4.2)] where we add multiple of the identity to the (1,1) and (2,2) blocks,

$$(5.20) \quad \begin{bmatrix} \vec{\mathbf{B}}^{(\ell)} + \delta \mathbf{I} & \vec{\mathbf{A}}^{(\ell)\top} \\ \vec{\mathbf{A}}^{(\ell)} & -\gamma^{(\ell)} \mathbf{I} \end{bmatrix} \begin{bmatrix} \vec{\mathbf{d}}^{(\ell)} \\ \vec{\mathbf{w}}^{(\ell)} \end{bmatrix} = \begin{bmatrix} -\vec{\mathbf{g}}^{(\ell)} \\ \vec{\mathbf{A}}^{(\ell)} \vec{\mathbf{p}}^{(\ell)} \end{bmatrix}.$$

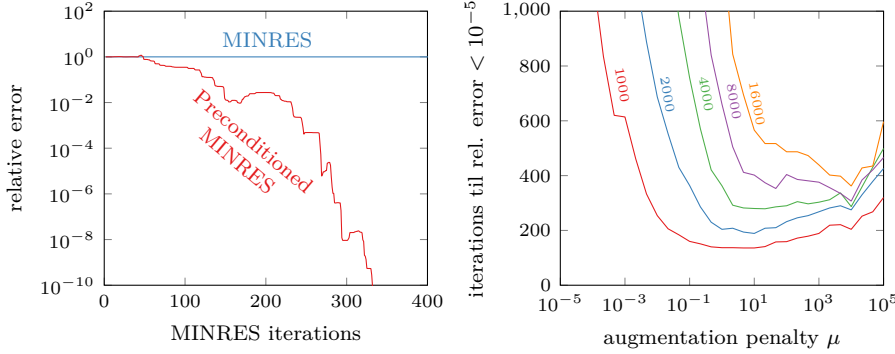


FIG. 5.1. The preconditioner \mathcal{M} accelerates the convergence of MINRES on the KKT system (5.20). On the left we show the convergence of the solution on a problem with $m = 4000$ and $\mu = 100$, where relative error refers to the mismatch between the iterate's solution and the converged value. On the right, note the number of MINRES solutions required varies as a function of augmentation penalty μ and problem dimension m . This example uses data from the Van der Pol oscillator described in subsection 6.1.3.

In our implementation we fix $\delta = 10^{-4}$ and scale γ based on the previous iteration

$$(5.21) \quad \gamma^{(\ell)} = 10^{-4} \left(\|\vec{\mathbf{g}}^{(\ell-1)} + \vec{\mathbf{w}}^{(\ell-1)} \vec{\mathbf{A}}^{(\ell-1)}\|_1 + \|\vec{\mathbf{h}}^{(\ell-1)}\|_1 \right).$$

To solve (5.20), we use a preconditioned MINRES iteration following Alger, et al. [1]. This preconditioner is derived from a block-diagonal approximation of the KKT system corresponding the augmented objective,

$$(5.22) \quad f_\mu(\vec{\mathbf{c}}, \vec{\mathbf{z}}) := f(\vec{\mathbf{c}}, \vec{\mathbf{z}}) + \mu \|\vec{\mathbf{h}}(\vec{\mathbf{c}}, \vec{\mathbf{w}})\|_2^2$$

for some penalty $\mu > 0$. In our setting, this preconditioner is

$$(5.23) \quad \mathcal{M}^{(\ell)} = \begin{bmatrix} \alpha \vec{\mathbf{W}} + \delta \mathbf{I} + \mu \vec{\mathbf{K}}^{(\ell)\top} \vec{\mathbf{K}}^{(\ell)} & \\ & \vec{\mathbf{M}} + \delta \mathbf{I} + \mu \vec{\mathbf{L}}^{(\ell)\top} \vec{\mathbf{L}}^{(\ell)} \\ & & \frac{1}{\mu} \mathbf{I} \end{bmatrix}.$$

We efficiently apply $\mathcal{M}^{(\ell)-1}$ blockwise. The first block is small, dn , so we explicitly compute its inverse. The second block is large, dm , but low bandwidth $dq \ll dm$, so we apply its inverse by precomputing a sparse factorization; in our experiments an LU factorization computed using SuperLU [13]. As illustrated in Figure 5.1, this preconditioner enables rapid solution of the KKT system. In our setting, the performance of this preconditioner depends on augmentation penalty μ . As these experiments show, a value $\mu \in [10, 1000]$ enables fast convergence for a variety of problem dimensions; our experiments take $\mu = 100$.

5.3. Multiple Trajectories. In some situations it is necessary incorporate data from multiple trajectories to ensure the operator inference problem is well posed [33]. For example, a single trajectory might not sufficiently explore the state-space to enable an accurate estimate of the parameters $\vec{\mathbf{c}}$. Fortunately, SIDDS can be easily modified to accommodate this situation. Suppose we have trajectories $\{\vec{\mathbf{y}}_{(i)}\}_{i=1}^T$, we then seek

to solve an extension of (5.1)

$$(5.24) \quad \min_{\vec{c}, \vec{z}_{(1)}, \dots, \vec{z}_{(T)}} \sum_{t=1}^T \frac{1}{2} [\vec{y}_{(t)} - \vec{z}_{(t)}]^\top \vec{M}_{(t)} [\vec{y}_{(t)} - \vec{z}_{(t)}] + \frac{\alpha}{2} \vec{c}^\top \vec{W} \vec{c},$$

$$\text{s.t. } \vec{D}_p \vec{z}_{(i)} - \vec{\Phi}(\vec{z}_{(i)}) \vec{c} = \mathbf{0} \quad t = 1, \dots, T.$$

Structurally, this optimization problem is similar to (5.1) enabling us to use the same techniques to efficiently solve this problem. Using similar notation as before, the constraint derivative with respect to each trajectory i has components

$$(5.25) \quad \vec{K}_{(i)}^{(\ell)} := -\vec{\Phi}(\vec{z}_{(i)}^{(\ell)}) \quad \vec{L}_{(i)}^{(\ell)} := \vec{D}_p - [\nabla \vec{\Phi}(\vec{z}_{(i)}^{(\ell)}) \bar{\times}_2 \vec{c}^{(\ell)}].$$

We can then combine these to form the full constraint derivative

$$(5.26) \quad \vec{A}^{(\ell)} := \begin{bmatrix} \vec{K}_{(1)}^{(\ell)} & \vec{L}_{(1)}^{(\ell)} & & \\ \vdots & & \ddots & \\ \underbrace{\vec{K}_{(T)}^{(\ell)}}_{\vec{K}_{\square}^{(\ell)}} & \underbrace{\vec{L}_{(T)}^{(\ell)}}_{\vec{L}_{\square}^{(\ell)}} & & \end{bmatrix}$$

These two matrices $\vec{K}_{\square}^{(\ell)}$ and $\vec{L}_{\square}^{(\ell)}$ with dense rectangular block and a sparse, low-bandwidth square matrix can be used analogously in place of $\vec{K}^{(\ell)}$ and $\vec{L}^{(\ell)}$ in the preceding analysis for the relaxation step and the quadratic subproblem. This enables an efficient solution to SIDDS with multiple trajectory data.

6. Examples. In this section we provide a few examples illustrating the performance of SIDDS and comparing against existing methods on three representative test problems. In each case, we use basis functions $\{\phi_k\}_k$ corresponding to a degree- p total-degree monomial basis,

$$(6.1) \quad \mathcal{P}_n^p := \{\phi_{\alpha}(\mathbf{x})\}_{|\alpha| \leq p}, \quad \phi_{\alpha}(\mathbf{x}) = \prod_{i=1}^n x_i^{\alpha_i}, \quad |\alpha| := \sum_{i=1}^n \alpha_i$$

where $\alpha \in \mathbf{Z}_+^d$ is a multi-index over d nonnegative integers. Unless otherwise mentioned, we use the smallest basis that includes the desired differential equation.

6.1. Test Problems. Here we consider three common test problems the Duffing oscillator, Lorenz 63 attractor, and the Van der Pol Oscillator; see, e.g., [6, 9, 21]. We focus on these low-dimensional problems where we can perform Monte Carlo tests to evaluate performance over multiple realizations of noise. Unless otherwise mentioned, we use the time step $\delta = 10^{-2}$. To generate measurements \vec{y} , we first evolve the corresponding differential equation using SciPy's `solve_ivp` with the DOP853 integrator to generate \vec{y} . Then to generate noisy measurements, we sample $\vec{n} \sim \mathcal{N}(\vec{0}, \vec{\Sigma})$ and form $\vec{y} = \vec{x} + \vec{n}$.

6.1.1. Duffing Oscillator. The Duffing oscillator models a nonlinear pendulum; here we considered a damped variant where

$$(6.2) \quad \begin{cases} \dot{x}_1 = x_2, & x_1(0) = -2, \\ \dot{x}_2 = -0.1x_2 - x_1 - 5x_1^3, & x_2(0) = -2. \end{cases}$$

In our experiments, we typically use $m = 1000$ measurements of this system.

6.1.2. Lorenz 63 Attractor. The Lorenz 63 attractor is a chaotic system developed initially from models of atmospheric convection:

$$(6.3) \quad \begin{cases} \dot{x}_1 = 10(x_2 - x_1), & x_1(0) = -8, \\ \dot{x}_2 = x_1(28 - x_3) - x_2, & x_2(0) = 7, \\ \dot{x}_3 = x_1x_2 - \frac{8}{3}x_3, & x_3(0) = -28. \end{cases}$$

In our experiments, we typically use $m = 2000$ measurements of this system.

6.1.3. Van der Pol Oscillator. The Van der Pol oscillator is a nonlinear ODE with a non-trivial limit cycle

$$(6.4) \quad \begin{cases} \dot{x}_1 = x_2, & x_1(0) = 0, \\ \dot{x}_2 = 2x_2(1 - x_1^2) - x_1, & x_2(0) = 1. \end{cases}$$

In our experiments, we typically use $m = 1000$ measurements of this system.

6.2. SIDDS+ ℓ_0 Convergence. To begin, we consider SIDDS+ ℓ_0 and show how the IRLS approximation of the regularization affects the convergence history. Figure 6.1 shows how several quantities perform as a function of iteration number in the Lorenz 63 example with $m = 2000$ measurements, sample rate $\delta = 10^{-2}$, and noise $\vec{n} \sim \mathcal{N}(\vec{0}, \sigma^2 \mathbf{I})$ where $\sigma = 0.1$. We note that even with large IRLS regularization $\epsilon = 1$ in the first few iterates, the SQP solver quickly approximates the state in \vec{z} and satisfies the constraint to 10^{-5} within 13 iterations. Subsequently, as we decrease the IRLS regularization we slowly obtain better coefficient estimates while still satisfying the equality constraints. After taking $\epsilon = 10^{-8}$, we perform a few SQP iterations where the discovered sparsity structure is fixed to remove the bias introduced by the ℓ_0 regularization; this is labeled ‘polish.’

6.3. Derivative Approximation. An important hyperparameter determining the accuracy of SIDDS is the order of the finite difference approximation. Choosing this parameter, it is important to find a middle ground—a low order approximation makes \vec{h} a poor approximation of the continuous dynamical system constraint, but a high order approximation increases computational cost and has small coefficients that can yield cancellation errors. Figure 6.2 shows how different central finite difference stencils affect the accuracy of \vec{c} as estimated by SIDDS. Here we see that a 9-point central finite difference estimate allows the highest time step δ without losing accuracy. We use this 9-point scheme (8th order accurate) in the rest of our examples.

6.4. Virtual Measurements. Another approach to improve the accuracy of the derivative approximation is to add *virtual* measurements between our actual measurements to decrease the effective sample rate δ . For example, we can half the sample rate by adding virtual measurements after every actual measurement, setting

$$(6.5) \quad \vec{y} = [\mathbf{y}_1^\top \quad \mathbf{0} \quad \mathbf{y}_2^\top \quad \mathbf{0} \quad \cdots \quad \mathbf{y}_m^\top]^\top, \quad \vec{\mathbf{M}} = \text{diag}(\mathbf{I}_d, \mathbf{0}_d, \mathbf{I}_d, \mathbf{0}_d, \cdots, \mathbf{I}_d),$$

where \mathbf{I}_d and $\mathbf{0}_d$ are the $d \times d$ identity and zeros matrices. We refer this variant by how the dimensions of the problem increase; e.g., (6.5) is SIDDS-2 \times . As Figure 6.3 illustrates, this approach allows us to resolve data with a slower sample rate than standard SIDDS. With standard SIDDS, we are able to accurately recover coefficients for $\delta \lesssim 0.08$; but with SIDDS-2 \times , $\delta \lesssim 0.15$, and SIDDS-16 \times , $\delta \lesssim 0.8$. Since our Van der Pol oscillator has a limit cycle with period 7.63, SIDDS-16 \times is recovering the system with only ~ 10 measurements per period.

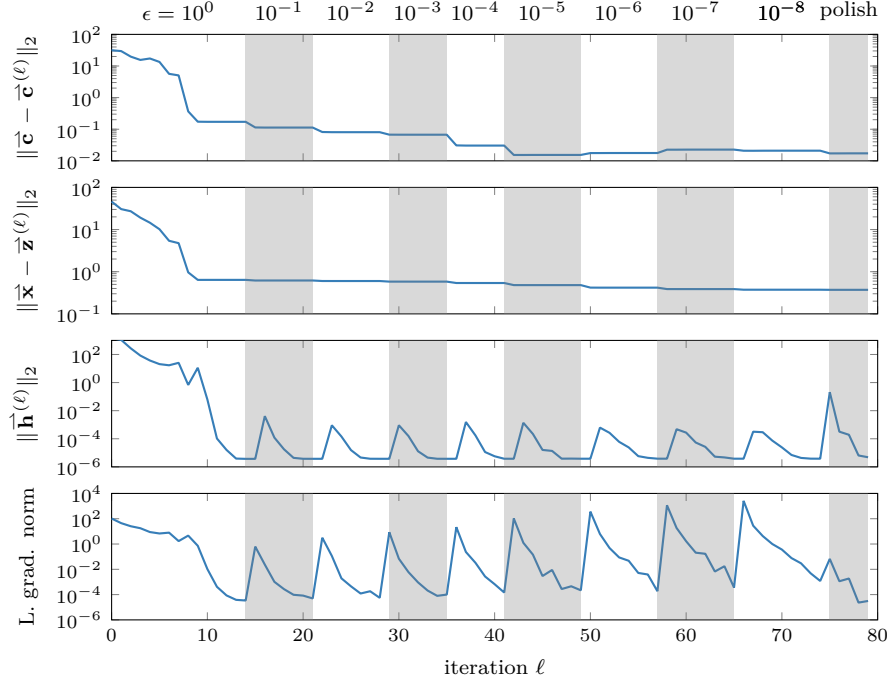


FIG. 6.1. The convergence of $SIDS+\ell_0$ solved using an IRLS approach. Stripes denote the different values of ϵ used as regularization of the IRLS approximation of the ℓ_0 -norm. The bottom plot shows the norm of the gradient of the Lagrangian, $\|\vec{\mathbf{g}}^{(\ell)} + \vec{\mathbf{A}}^{(\ell)\top} \vec{\mathbf{w}}^{(\ell)}\|_2$. The data for this problem corresponds to the Lorenz 63 attractor example with added noise with standard deviation $\sigma = 0.1$. Note the dynamical system evolution constraint is satisfied to approximately 10^{-5} .

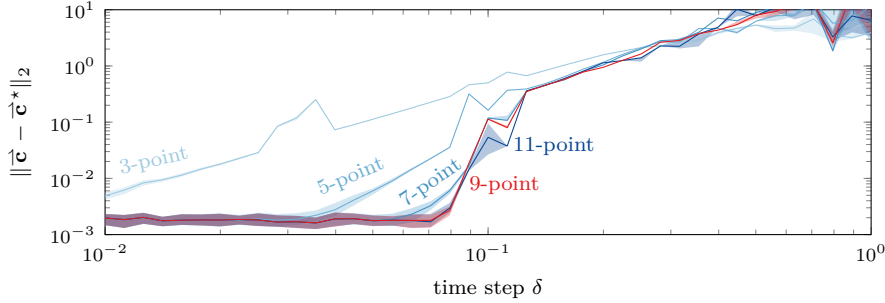


FIG. 6.2. Performance of multiple central finite difference derivative approximations on the solution generated by SIDS. In this example we collect $m = 1000$ data points of the Van der Pol system starting from a point on the limit cycle and vary the time step δ . This example has noise with standard deviation $\sigma = 10^{-2}$; the shaded region represents the 25th to 75th percentiles from 100 trials.

6.5. Multiple Trajectories. As noted by Wu and Xiu [33], multiple trajectories are sometimes necessary to make estimating the dynamical system well posed. Here we consider their example 3 without noise,

$$(6.6) \quad \begin{cases} \dot{x}_1 = x_1(1 - x_1 - x_2), \\ \dot{x}_2 = x_2(0.5 - 0.25x_2 - 0.75x_1). \end{cases}$$

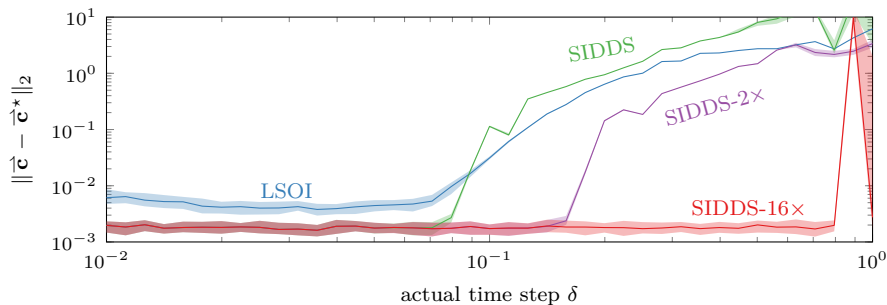


FIG. 6.3. Increasing the number of samples in the constraint, we are able better recover the dynamical system with slow sampling rates δ . Here SIDDs-2 \times and SIDDs-16 \times refer to increasing the number of points used to evolve the dynamics in the constraint (but not the data) by two and sixteen times. This uses the same example as in Figure 6.2.

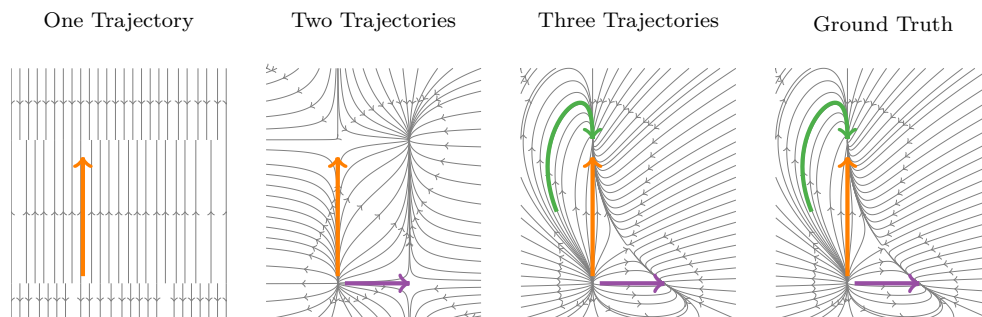


FIG. 6.4. Streamline plots resulting from identifying the dynamical system in (6.6); the thick, colored lines denote the measured trajectory data.

As illustrated in Figure 6.4, if the trajectories are not sufficiently informative we cannot estimate the dynamical system. However, with sufficient trajectories we are able to exactly recover the dynamical system.

6.6. Increasing Data. A typical statistical question is: how does a method perform with increasing amounts of data? Figure 6.5 provides an example answering this question for SIDDs and LSOI the Lorenz 63 example with noise with standard deviation $\sigma = 10^{-2}$. This example shows the estimates provided by SIDDs are an order of magnitude better than LSOI and that LSOI requires two orders of magnitude more data to obtain a similar accuracy to SIDDs. Moreover, this example shows SIDDs can scale to large problems.

6.7. Correlated Noise. With SIDDs, we can also incorporate knowledge of noise correlation. Suppose that noise \mathbf{n}_j at time j is correlated between coordinates with correlation $\rho \in [0, 1)$:

$$(6.7) \quad \mathbf{n}_j \sim \mathcal{N}\left(\mathbf{0}, \sigma^2 \begin{bmatrix} 1 & \rho \\ \rho & 1 \end{bmatrix}\right), \text{ if } \mathbf{n}_j \in \mathbb{R}^2; \quad \mathbf{n}_j \sim \mathcal{N}\left(\mathbf{0}, \sigma^2 \begin{bmatrix} 1 & \rho & 0 \\ \rho & 1 & 0 \\ 0 & 0 & 1 \end{bmatrix}\right), \text{ if } \mathbf{n}_j \in \mathbb{R}^3.$$

Then $\vec{\mathbf{n}} \sim \mathcal{N}(\vec{\mathbf{0}}, \vec{\Sigma})$ where $\vec{\Sigma}$ is a block diagonal matrix consisting of m repetitions of the block above. Taking weight $\vec{\mathbf{M}} = \vec{\Sigma}^{-1}$ in SIDDs, we obtain near optimal estimates as shown in Figure 6.6.

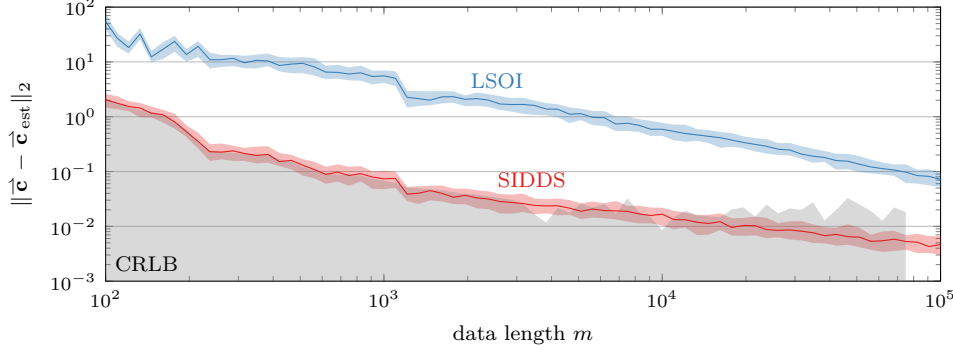


FIG. 6.5. As the quantity of data increases in the Lorenz 63 example with noise $\sigma = 10^{-2}$, both SIDDS and LSOI obtain better coefficient estimates. SIDDS is able to approximately obtain the Cramér-Rao lower bound (CRLB) denoted by the shaded region; since this system is chaotic, we are unable to accurately compute this bound for large m .

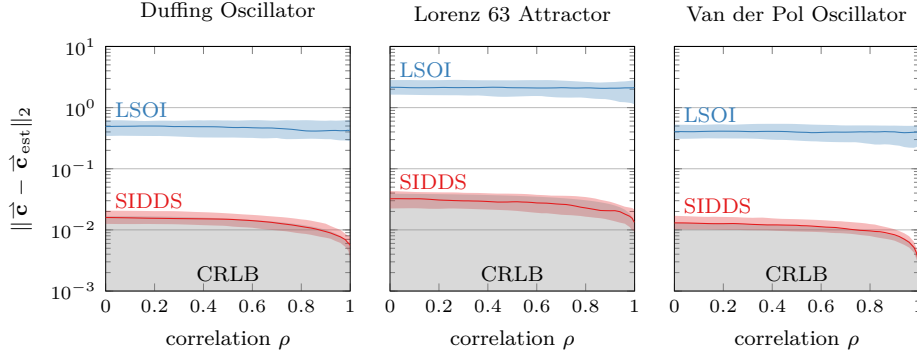


FIG. 6.6. Here we illustrate how SIDDS performs on correlated noise as described in (6.7) with $\sigma = 10^{-2}$. Because SIDDS accounts for the correlation, it obtains estimates that approximately satisfies the lower bound.

6.8. Comparing SIDDS to Other Algorithms. Finally, we compare SIDDS to other algorithms for estimating dynamical systems from measurements. We separate these algorithms into two classes: those with and without a sparsity promoting constraint. Without a sparsity promoting constraint, we compare SIDDS and LSOI. With a sparsity promoting constraint, we compare SIDDS+ ℓ_0 with SINDy using STLS as implemented in PySINDy [12, 23], and Modified SINDy (mSINDy) as implemented by [21]. These comparisons are shown in Figure 6.7 using the standard conditions mentioned in subsection 6.1 with additive i.i.d. noise $\bar{\mathbf{n}} \sim \mathcal{N}(\mathbf{0}, \sigma^2 \mathbf{I})$.

Both LSOI and SIDDS have no free parameters, but the sparsity promoting algorithms have several hyperparameters that need to be tuned to obtain an accurate solution. For STLS, we used the default parameters in PySINDy. For mSINDy, we used the parameters in their numerical experiments for the corresponding test problem: truncation parameter λ of 0.05, 0.2, and 0.1 and ADAM steps per outer iteration of 5000, 15000, and 5000 for Duffing, Lorenz 63, and Van der Pol respectively. For SIDDS+ ℓ_0 , we choose the penalty α of 0.01, 0.5, and 1 respectively, via a coarse optimization to maximize the probability of recovering the correct sparsity structure in the limit of large noise.

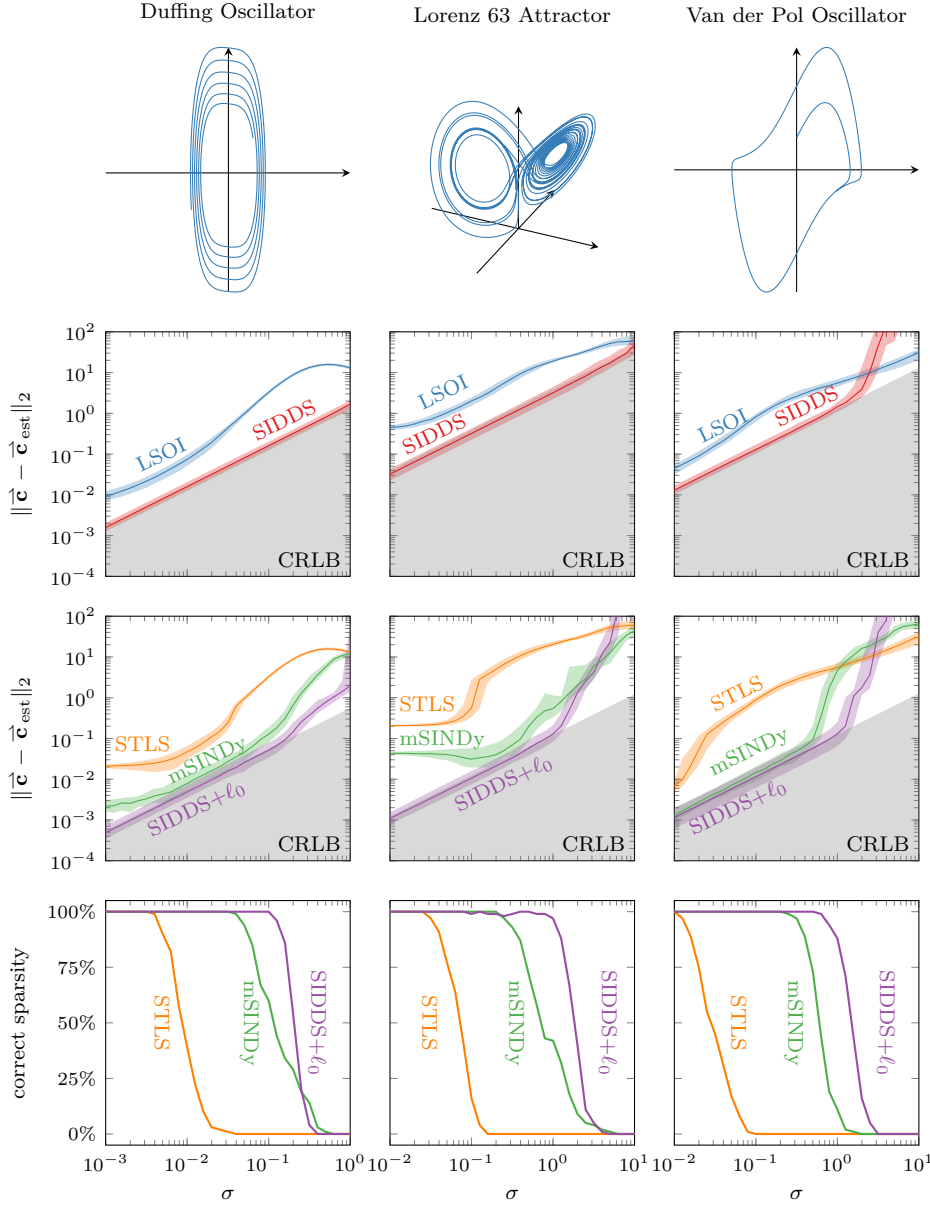


FIG. 6.7. The accuracy of various methods for recovering the coefficients and sparsity pattern of three different dynamical systems with increasing standard deviation of measurement noise σ . In these examples, the time step was fixed at $\delta = 10^{-2}$ and 100 trials performed for each value of σ . Shaded regions enclose the 25th to 75th percentile of results. Gray shaded regions indicate the accuracy excluded by the Cramér-Rao bound.

The experiments shown in Figure 6.7 illustrate several key points. First, SIDDs and SIDDs+ ℓ_0 approximately obtain the Cramér-Rao lower bound for small noise σ ; for large noise, these algorithms identify a local minimizer far away the true solution leading the estimates to detach from the lower bound. Second, the denoising penalty introduced by mSINDy does yield better estimates than STLS SINDy, it does not

obtain the lower bound. Third, SIDDS+ ℓ_0 is able to correctly identify the sparsity structure for larger noise than STLS and mSINDy.

7. Discussion. Here we have shown how to simultaneously identify and denoise dynamical systems using SIDDS and its sparsity promoting variant SIDDS+ ℓ_0 . Unlike existing work, SIDDS poses the dynamical system evolution as an equality constraint rather than as a penalty. This enables SIDDS to outperform several existing algorithms for identifying dynamical systems from noisy measurements and approximately obtain the Cramér-Rao lower bound for small noise. For brevity, we have used a simple smoothing approach for initializing SIDDS; however, performance in the large noise regime can likely be improved using techniques discussed in [10].

The inverse problem perspective and solution framework used by SIDDS provides a new avenue for related problems that identifying dynamical systems from noisy measurements. For example: systems with higher order dynamics, e.g., $\ddot{\mathbf{x}}(t) = \mathbf{f}(\mathbf{x}, \dot{\mathbf{x}}; \mathbf{C})$; systems with nonautonomous input $\mathbf{u}(t)$ as in [22], e.g., $\dot{\mathbf{x}}(t) = \mathbf{f}(\mathbf{x}; \mathbf{C}) + \mathbf{u}(t)$; systems with hidden variables, e.g., when measurements \mathbf{y}_j have fewer elements than \mathbf{x} ; and those with parameterized basis functions, e.g., $\mathbf{f}(\mathbf{x}; \mathbf{C}, \boldsymbol{\theta}) = \sum_k \mathbf{c}_k \phi_k(\mathbf{x}, \boldsymbol{\theta})$. We anticipate approaching these problems in future work.

REFERENCES

- [1] N. ALGER, U. VILLA, T. BUI-THANH, AND O. GHATTAS, *A data scalable augmented Lagrangian KKT preconditioner for large-scale inverse problems*, SIAM J. Sci. Comput., 39 (2017), pp. A2365–A2393, <https://doi.org/10.1137/16m1084365>.
- [2] M. ASCH, M. BOCQUET, AND M. NODET, *Data Assimilation*, Society for Industrial and Applied Mathematics, Dec. 2016, <https://doi.org/10.1137/1.9781611974546>.
- [3] Z. BEN-HAIM AND Y. C. ELDAR, *On the constrained Cramér–Rao bound with a singular Fisher information matrix*, IEEE Signal Process. Lett., 16 (2009), pp. 453–456, <https://doi.org/10.1109/lsp.2009.2016831>.
- [4] Å. BJÖRCK, *Numerical Methods for Least Squares Problems*, SIAM, Philadelphia, PA, 1996.
- [5] T. BLUMENSATH AND M. E. DAVIES, *Iterative hard thresholding for compressed sensing*, Appl. Comput. Harmon. A., 27 (2009), pp. 265–274, <https://doi.org/10.1016/j.acha.2009.04.002>.
- [6] S. L. BRUNTON, J. L. PROCTOR, AND J. N. KUTZ, *Discovering governing equations from data by sparse identification of nonlinear dynamical systems*, Proc. Natl. Acad. Sci. USA, 113 (2016), pp. 3932–3937.
- [7] E. J. CANDÈS, M. B. WAKIN, AND S. P. BOYD, *Enforcing sparsity by reweighted ℓ_1 minimization*, J. Fourier Anal. Appl., 14 (2008), pp. 877–905, <https://doi.org/10.1007/s00041-008-9045-x>.
- [8] R. CHARTRAND AND W. YIN, *Iteratively reweighted algorithms for compressive sensing*, in 2008 IEEE International Conference on Acoustics, Speech and Signal Processing, IEEE, Mar. 2008, <https://doi.org/10.1109/icassp.2008.4518498>.
- [9] A. CORTIELLA, K.-C. PARK, AND A. DOOSTAN, *Sparse identification of nonlinear dynamical systems via reweighted ℓ_1 -regularized least squares*, Comput. Method. Appl. M., 376 (2021), p. 113620, <https://doi.org/10.1016/j.cma.2020.113620>.
- [10] A. CORTIELLA, K.-C. PARK, AND A. DOOSTAN, *A priori denoising strategies for sparse identification of nonlinear dynamical systems: A comparative study*, 2022, <https://arxiv.org/abs/2201.12683v1>.
- [11] I. DAUBECHIES, R. DEVORE, M. FORNASIER, AND C. S. GÜNTÜRK, *Iteratively reweighted least squares minimization for sparse recovery*, Comm. Pure Appl. Math., 63 (2010), pp. 1–38, <https://doi.org/10.1002/cpa.20303>.
- [12] B. DE SILVA, K. CHAMPION, M. QUADE, J.-C. LOISEAU, J. KUTZ, AND S. BRUNTON, *PySINDy: A python package for the sparse identification of nonlinear dynamical systems from data*, JOSS, 5 (2020), p. 2104, <https://doi.org/10.21105/joss.02104>, <https://doi.org/10.21105/joss.02104>.
- [13] J. W. DEMMEL, S. C. EISENSTAT, J. R. GILBERT, X. S. LI, AND J. W. H. LIU, *A supernodal approach to sparse partial pivoting*, SIAM J. Matrix Anal. & Appl., 20 (1999), pp. 720–755, <https://doi.org/10.1137/s0895479895291765>.
- [14] G. H. GOLUB AND V. PEREYRA, *The differentiation of pseudo-inverses and nonlinear least*

- squares problems whose variables separate, *SIAM J. Numer. Anal.*, 10 (1973), pp. 413–432, <https://doi.org/10.1137/0710036>.
- [15] G. H. GOLUB AND C. F. VAN LOAN, *Matrix Computations*, Johns Hopkins University Press, Baltimore, MD, fourth ed., 2013.
 - [16] E. HABER AND U. M. ASCHER, *Preconditioned all-at-once methods for large, sparse parameter estimation problems*, *Inverse Probl.*, 17 (2001), pp. 1847–1864, <https://doi.org/10.1088/0266-5611/17/6/319>.
 - [17] E. HABER, U. M. ASCHER, AND D. OLDENBURG, *On optimization techniques for solving nonlinear inverse problems*, *Inverse Probl.*, 16 (2000), pp. 1263–1280, <https://doi.org/10.1088/0266-5611/16/5/309>.
 - [18] M. HEINKENSCHLOSS, *Numerical solution of implicitly constrained optimization problems*, Tech. Report TR08-05, Rice University, 2013, <https://hdl.handle.net/1911/102087>.
 - [19] R. A. HORN AND C. R. JOHNSON, *Matrix Analysis*, Cambridge University Press, Cambridge, 1985, <https://doi.org/10.1017/CBO9780511810817>.
 - [20] R. A. HORN AND C. R. JOHNSON, *Matrix Analysis*, Cambridge University Press, 2009, <https://doi.org/10.1017/cbo9781139020411>.
 - [21] K. KAHAMAN, S. L. BRUNTON, AND J. N. KUTZ, *Automatic differentiation to simultaneously identify nonlinear dynamics and extract noise probability distributions from data*, 2020, <https://arxiv.org/abs/2009.08810v2>.
 - [22] E. KAISER, J. KUTZ, AND S. BRUNTON, *Sparse identification of nonlinear dynamics for model predictive control in the low-data limit*, *Proc. R. Soc. A.*, 474 (2018), p. 20180335, <https://doi.org/10.1098/rspa.2018.0335>, <https://doi.org/10.1098/rspa.2018.0335>.
 - [23] A. A. KAPTANOGLU, B. M. DE SILVA, U. FASEL, K. KAHAMAN, A. J. GOLDSCHMIDT, J. L. CALLAHAM, C. B. DELAHUNT, Z. G. NICOLAOU, K. CHAMPION, J.-C. LOISEAU, J. N. KUTZ, AND S. L. BRUNTON, *Pysindy: A comprehensive python package for robust sparse system identification*, arXiv preprint arXiv:2111.08481, (2021).
 - [24] T. G. KOLDA AND B. W. BADER, *Tensor decompositions and applications*, *SIAM Rev.*, 51 (2009), pp. 455–500, <https://doi.org/10.1137/07070111X>.
 - [25] M.-J. LAI, Y. XU, AND W. YIN, *Improved iteratively reweighted least squares for unconstrained smoothed ℓ_q minimization*, *SIAM J. Numer. Anal.*, 51 (2013), pp. 927–957, <https://doi.org/10.1137/110840364>.
 - [26] X. LIU AND Y. YUAN, *A sequential quadratic programming method without a penalty function or a filter for nonlinear equality constrained optimization*, *SIAM J. Optim.*, 21 (2011), pp. 545–571, <https://doi.org/10.1137/080739884>.
 - [27] B. PEHERSTOFER AND K. WILLCOX, *Data-driven operator inference for nonintrusive projection-based model reduction*, *Comput. Methods Appl. Mech. Engrg.*, 306 (2016), pp. 196–215, <https://doi.org/10.1016/j.cma.2016.03.025>.
 - [28] S. H. RUDY, J. N. KUTZ, AND S. L. BRUNTON, *Deep learning of dynamics and signal-noise decomposition with time-stepping constraints*, *J. Comput. Phys.*, 396 (2019), pp. 483–506, <https://doi.org/10.1016/j.jcp.2019.06.056>.
 - [29] G. A. F. SEBER AND C. J. WILD, *Nonlinear Regression*, Wiley-Interscience, 1989.
 - [30] F. SUN, Y. LIU, AND H. SUN, *Physics-informed spline learning for nonlinear dynamics discovery*, in Proceedings of the Thirtieth International Joint Conference on Artificial Intelligence, International Joint Conferences on Artificial Intelligence Organization, Aug. 2021, <https://doi.org/10.24963/ijcai.2021/283>.
 - [31] G. TRAN AND R. WARD, *Exact recovery of chaotic systems from highly corrupted data*, *Multi-scale Model. Simul.*, 15 (2017), pp. 1108–1129, <https://doi.org/10.1137/16m1086637>.
 - [32] S. J. WRIGHT, *An algorithm for degenerate nonlinear programming with rapid local convergence*, *SIAM J. Optim.*, 15 (2005), pp. 673–696, <https://doi.org/10.1137/030601235>.
 - [33] K. WU AND D. XIU, *Numerical aspects for approximating governing equations using data*, *J. Comput. Phys.*, 384 (2019), pp. 200–221, <https://doi.org/10.1016/j.jcp.2019.01.030>, <https://doi.org/10.1016/j.jcp.2019.01.030>.